COMPUTATIONAL ANALYSIS OF A SOLAR VORTEX

A THESIS SUBMITTED TO
THE BOARD OF CAMPUS GRADUATE PROGRAMS
OF MIDDLE EAST TECHNICAL UNIVERSITY
NORTHERN CYPRUS CAMPUS

BY

ABDULLAH MOHIUDDIN

IN PARTIAL FULLFILLMENT OF THE REQUIREMENTS
FOR
THE DEGREE OF MASTER OF SCIENCE
IN
SUSTAINABLE ENVIRONMENT AND ENERGY SYSTEMS

MARCH 2015

Approval of the Board of Graduate Programs

_____
Prof. Dr. Tanju Mehmetoğlu
Chairperson

I certify that this thesis satisfies all the requirements as a thesis for the degree of Master of Science.

_____
Assoc. Prof. Dr. Ali Muhtaroğlu
Program Coordinator

This is to certify that we have read this thesis and that in our opinion it is fully adequate, in scope and quality, as a thesis for the degree of Master of Science.

_____
Assoc. Prof. Dr. Eray Uzgoren
Supervisor

Examining Committee Members

Assoc. Prof. Dr. Eray Uzgören	Mechanical Engineering Dept. METU NCC	_____
Prof. Dr. M. Cevdet Celenligil	Aerospace Engineering Dept. METU NCC	_____
Assoc. Prof. Dr. Derek Baker	Mechanical Engineering Dept. METU Ankara	_____

I hereby declare that all information in this document has been obtained and presented in accordance with academic rules and ethical conduct. I also declare that, as required by these rules and conduct, I have fully cited and referenced all material and results that are not original to this work.

Name, Last name : Abdullah Mohiuddin

Signature :

ABSTRACT

COMPUTATIONAL ANALYSIS OF A SOLAR VORTEX

Abdullah Mohiuddin

M.S., Sustainable Environment and Energy Systems Program

Supervisor: Assoc. Prof. Dr. Eray Uzgoren

March 2015, 73 Pages

This thesis investigates power generation opportunities by considering computational analysis of an experimental setup which is initially proposed to mimic dust devils in a controlled environment. The concept relies on buoyancy effect over a heated plate surrounded by vertical thin plates or vanes. Once the heated air starts rising, vertical vanes help surrounding air to flow inwards in a direction tangential to the vortex core to introduce swirl to the flow. Present study focuses on the computational fluid dynamics based analysis of a meter scale experimental setup using OpenFOAM. First, the developed model is validated against experimental data available in the literature and theoretical models developed for naturally occurring dust devils. The novelty of the thesis is that it is the first parametric study that investigates the effects of the number of vanes, vane angles, vane height, vane width, on axial volumetric flow rate profiles of the experimental setup. It is found that axial flow rate increases with vane height, while there exists an optimal vane width and vane spacing to enhance axial flow rate. It is also found that an increase in vane angles only from 25º to 40º improves the mass flow rate while reducing below 25º or increasing above 40º does not change the mass flow rate significantly. On the other, amount of swirl is found to increase continuously with the vane angle which suggests that various turbine blade geometries can be considered to optimize power harvesting opportunities.

Keywords: Renewable Energy, Dust devils, Natural Convection, solar vortex

ÖZ

GÜNEŞ GİRDABININ HESAPLAMALI ANALİZİ

Abdullah Mohiuddin
Yüksek Lisans, Sürdürülebilir Çevre ve Enerji Sistemleri Programı
Tez Yöneticisi: Doç. Dr. Eray Uzgoren
Mart 2015, 73 sayfa

Bu tez, toz hortumlarını kontrollü bir ortamda araştırmak üzere tasarlanmış bir deney bır deney duzenegının hesaplamalı analız yontem kullanarak güç elde etme olanaklarını araştırır. Düzeneğin özelliği, ısıtılmış bir yüzey üzerinden yükselen havanın, yüzeyin çevresine yerleştirilmiş dikey ince plakalar veya kanatlar sayesinde dışarıdan gelen havanın bir açı ile içeriye akmasını ve dolayısıyla içerde yükselen havanın girdaba dönüşmesini sağlamasıdır. Bu deney düzeneğini incelemek üzere, hesaplamalı akışkanlar dinamiği yazılımı olan OpenFOAM kullanarak bir sayısal yöntem geliştirilmiştir. İlk olarak, geliştirilen yöntem; doğal yollardan oluşan toz hortumlarının diğer çalışmalarda bulunan deneysel verileri ve diğer geliştirilmiş çözümsel yöntemler ile karşılaştırılarak doğrulanmıştır. Tezin literatüre katkısı, bu sistemin oluşturacağı yükselme debisinin kanat açıları, kanat yüksekliği, kanat genişliği ve kanat sayısı ile değişiminin nitelendirmesidir. Yükselme debisini arttırmak için kanat genişliği ve aralığı için enuygun değerler olduğu bulunmuş ve kanat yüksekliğinin artmasının debiyi artırdığı sonucuna varılmıştır. Ayrıca kanat açısının 25º ile 40° arasında artırılması debiyi artırırken bu değerlerin altında veya üzerinde debide kaydadeğer değişim olmadığı bulunmuştur. Diğer yandan, girdap miktarı kanat açısı ile orantılı olarak değiştiği bulunmuş ve bunun farklı kanat kesitleri düşünülerek tasarlanacak türbinler için güç üretimi yapılabileceği gösterilmiştir.

DEDICATION

To my parents, my wife my brothers and sister.

For their unconditional support, trust and encouragement.

ACKNOWLEDGEMENTS

I want to offer my sincerest gratitude to my supervisor, Dr. Eray Uzgoren, who has supported me throughout my thesis with his patience and knowledge whilst providing me the room to work in my own way.

Besides my advisor, I would like to thank the other members of my thesis committee, Prof. Dr. M. Cevdet Celenligil, Asst. Prof. Dr. Derek Baker, for their insightful comments, and suggestions throughout the reviewing process.

I thank my fellow postgraduate students in Sustainable Environment and Energy Systems Program, Syed Zaid Hasany, Muhammad Azhar Ali Khan and Muhammad Arsalan Tariq for stimulating discussions and the friendly environment they provided throughout my research.

Finally I want to thank my wife and my parents and my siblings for their support and encouragement throughout my Masters.

TABLE OF CONTENTS

LIST OF TABLES

LIST OF FIGURES

NOMENCLATURE

R	Radius of the heated plate, (m)
h	Height of the vanes, (m)
c	Width of the vanes, (m)
$\boldsymbol{\Phi}$	Angular span
$\boldsymbol{\theta}$	Angle of vanes
T_P	Temperature of the heated plate, (k)
T_∞	Ambient temperature, (k)
ΔT	Temperature difference between ambient and heated plate
V_θ	Tangential velocity, (m/s)
V_r	Radial Velocity, (m/s)
V_Z	Vertical Velocity, (m/s)
r	Radial position (m)
z	Elevation (m)
g	gravity, (m/s^2)
R_a	Rayleigh number
β	Expansion co-efficient, (K^{-1})
υ	Kinematic viscosity, (N/s^2)
μ	Dynamic viscosity, (kg/ms)
Cp	Specific heat at constant pressure, (kJ/kg.K)
Pr	Prantal number
Gr	Grashof number
ρ	Density (kg/m^3)
V_f	Axial volumetric flow rate (m^3/s)
V_a	Average axial velocity (m/s)
S_w	Swirl number
V_c	Characteristic convective velocity (m/s)
V_{fc}	Characteristic convective volumetric flow rate (m^3/s)
V_{pa}	Peak averaged vertical velocity (m/s)
S	Geometric scaling factor

CHAPTER 1

1. INTRODUCTION

1.1. Introduction

The dust devil is a small sized vertical columnar vortex with high concentrations of kinetic energy, readily observed in the arid regions of the world. Length scale of a dust devil is depicted in terms of the radius of the vortex core which ranges from few meters to 60 meters reaching horizontal speeds of 10-20 m/s [1]. High kinetic energy potential of dust devils can provide new renewable power production opportunities, provided that their flow mechanism can be mimicked, deliberately controlled and anchored.

Despite dust devils' similarities to tornadoes in terms of flow features, its source of energy is not linked to latent heat as they can form in the absence of clouds. Dust devils' formation rather relies on the solar energy absorbed in the air near the surface which causes the formation of a thermal plume owing to buoyancy effects. Solar induced vertical flow alone is a necessary, but not an adequate condition for formation of dust devils as it requires a form of a vertical instability in the atmosphere [2]. It is not certain what conditions translates buoyancy induced upward flow into a columnar vortex, some authors suggested that thermal plumes can gain a sense of rotation from aerodynamic wake effects from surface roughness elements, which impart turbulence or vorticity on the airflow or from interaction of ground rolling cells or air [1][2] [6][7] , apart from that statistical data suggests that regions with strong solar potential, terrains with small rock cover but few trees, buildings, or grass, and gently sloping topography are listed as part of ideal conditions favoring dust devil formation [3].

Once formed, all dust devils exhibit several common features. The most visual feature is the vertical column which is the dust laden rotating mass with a height much larger than its width. The central region of this column is at an elevated temperature and at a lower pressure than ambient and is usually dust free. This region is referred as the core of a dust devil. Entrainment of dust particles happens at the base of the dust devil and they are carried vertically upward

while staying at the wall of the core due to centripetal acceleration based on the core radius r_c [1][2].

Due to its cylindrical shape, dust devils are usually considered in cylindrical coordinates .If seen vertically flow characteristics of a dust devil show differences that can be described in three distinct regions as shown in Figure 1.1[4]. The first region, just above the ground typically below 2 meters, is characterized by entrainment of surrounding air causing radial inflow toward vortex core at velocities exceeding the ambient wind speeds [1]. This region contains a stagnation point located near the center, where radial inflow is ceased before rotating and moving upward [1][2][6]. Second region contains both circulation and upward flow while no systematic radial flow is observed in the vortex core.

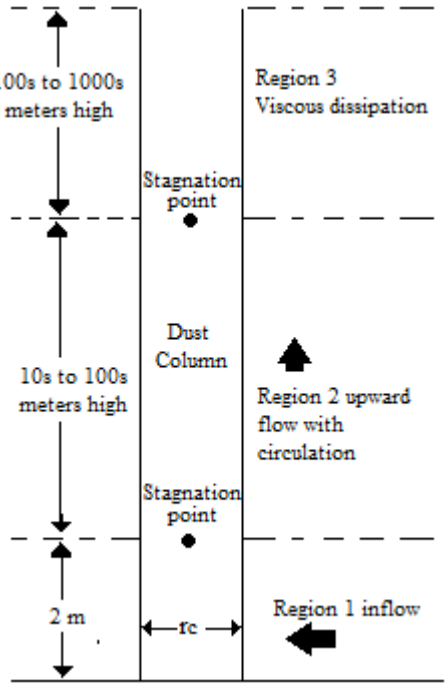

Figure 1.1 Regions within a dust devil

In some studies the tangential velocities in the first and second regions are represented by different vortex models including Rankine vortex model, Burgers-Rott vortex model and Lamb-Oseen vortex model. Tangential velocities increase typically from zero at the core center to $5 - 10\ m/s$ at the circumference of the core and decay inversely with the distance from the vortex core. It is noted by Tratt et al. [5] that this rate of decay vary with $r^{-1/2}$ in the first

region rather than r^{-1} probably owing to dominating viscous effects considering close proximity to the ground. Another feature of dust devil flows is associated with a second stagnation point, which is located above $2\,m$. This stagnation point is at the height where a central downdraft is present. In some dust devil flows this downdraft is stretched until the base of the vortex. [1], [6]. Finally, third region, beyond tens to hundreds of meters, is the dissipation zone where the vortex is weakened due to viscous effects.

The temperature difference between center of the vortex core and surrounding air is maximum in the first region, however no correlation is found so far between the maximum pressure drop and height [4]. Second region is typically warmed by the energy absorbed and carried by air and particles of the first region. This energy cascade has been considered by [7]–[9] in the development of a model treating a dust-devil as a heat engine that absorbs heat near the ground and discharges heat to air parcels subsiding outside the vortex by radiation. Their model describes a scaling relationship between measurable parameters through maximum temperature and pressure difference, and maximum tangential velocities of a dust devil. Predictions for peak tangential velocity agrees well with the measurements of [5] while the prediction of maximum temperature difference is yet to be confirmed due to lack of statistically valid number of measurements. Even though the model is promising on understanding dust devils, it requires that the air discharge height (length of third region) is known a priori which makes it difficult to use it for prediction purposes. Furthermore, the role of dust particles in this energy cascade is not clearly understood as in situ data by Lorenz and Myers [10] shows that there is volumetric solar heating of materials within the dust devil column, which suggests that the energy cascade can be more complicated than simply from the consideration that the thermal input is solely from the solar energy absorbed in the near surface layer.

Besides in situ measurements of dust devils, numerous studies are focused to form dust devil like vortices in laboratory environment or in numerical simulations. One of the early studies in the laboratory environment was performed by Fitzjarrald [11] in 1973 for the analysis of dust devil vortex through a device that is capable of mimicking the naturally occurring dust devils. Their experimental apparatus consisted of a circular, uniformly heated aluminum plate and 20 Plexiglas windows (vanes) around the circumference to impart tangential velocity component to the incoming air. A similar setup as shown in Figure 1.2 with differences in geometric

parameters such as number of vanes, radius and height was later considered by Simpson et al. [12] for exploring renewable power production opportunities. The working principle of both setups relies on the rise of heated air in the vertical direction from the heated plate in the region surrounded by these vanes. This convective plume at the center of the near ground surface causes an inward flow through the vanes, which directs the air to flow tangentially towards the center of the convective plume. The air acquires a velocity with tangential, axial and radial components.

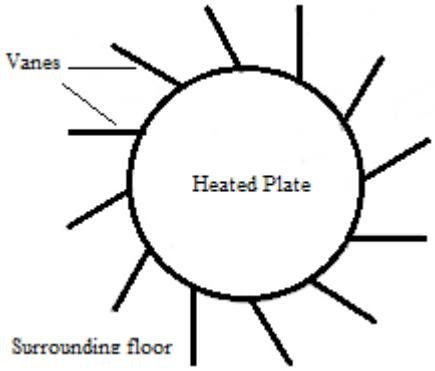

Figure 1.2 Top view of the experimental setup

Similar concept of a heated circular plate was considered in numerical simulations of formation of thermally driven vortices by Smith and Leslie [13] where they considered porous rotating screen instead of directional vanes to induce circulation. While there are other studies [27] [28] (Ward`s Chamber, Church et al.) utilizing the mechanical non-convective means to form tornado like vortices, but these lab models are not preferred by some researchers [11] for studying the dust-devil type vortex . These models often utilize an exhaust fan at the top to generate an updraft at the center of the vortex chamber and the fluid entrance is equipped with means to impart the swirl to onrushing fluid. This additional boundary at the top in the form of the exhaust fan is not present in the atmospheric vortices. The addition of this boundary at the top and absence of a thermal field makes it unsuitable for investigating features like thermal fields in dust devil-like vortices as it is suggested by Fitzjarrald [11]. The experimental setups that do not consider a heated plate include the Arizona State University Vortex Generator, ASUVG, have different motivation such as the role of particle entrainment by dust devils [14].

Above studies have shown that the energy cascade similar to a dust devil, can be captured, even in the absence of dusts and particles, by forming, anchoring and controlling the columnar vortices in a laboratory environment. Most of the abovementioned studies find motivation in understanding the flow mechanics of dust devils while only Simpson et al. [12] studied possibilities of power generation opportunities through such a system. The buoyancy-induced vortex setup consisted of a $4.8\ kW$ heated unit square plate surrounded by 12 planar aluminum vanes, each of which is $0.35\ m$ width and $0.6m$ height. They were able to demonstrate the formation of a vortex of $4\ m$ height, with surface core diameter of $5 - 25cm$. However, previous studies were not focused on how the system introduced by Fitzjarrald [11] and Simpson et al. [12] would be influenced by system parameters, i.e. characteristic radius of the heated plate, heat flux intensity, number of vanes, and vane dimensions.

The present study considers development of a numerical model of such a system with the view that it would be a promising renewable energy technology if solar energy can be utilized as a heat source as initial calculations by Simpson's et al. [12] predicted. Following chapter discusses the relevant background and previous works related to lab based and numerical experiments that are used to describe or mimic, the naturally occurring columnar vortices with a focus on the models utilizing heated surface as a source of updraft.

1.2. Thesis scope and structure

The power generation potential present in dust devil scale vortices can be tapped by developing an apparatus that could deliberately form similar atmospheric vortices. Studies are present in the literature discussing the field measurements and observations regarding the structure of naturally occurring dust devils [1][2][3].These studies which are briefly discussed in Chapter 2 provided a bench mark validation for the later numerical studies, some of which discuss the mechanisms of naturally occurring dust devils through simulations of natural physical environment with pre-decided boundary conditions[20][15]. Studies performed by Fitzjarrald, R.K Smith and Leslie, and Simpsons et al. included the use of experimental lab apparatus capable of mimicking the features present in dust devil scale vortices [11] [12] [13]. Present study is focused on the development and validation of the numerical model as described in chapter 3, to conduct investigations based on numerical simulations of the meter scale

experimental setup that can produce vortices similar to dust devils, using OpenFOAM, open source computational fluid dynamics software. First, a numerical model is developed followed by the validation study which is , as discussed in chapter 4, carried out using the experimental results of Simpsons et al. [12], and theoretical models such as Burgers-Rott vortex model, Rankine vortex model and Vatistas et al. for a comparison of features present in naturally occurring dust devils. After that a parametric study is included in chapter 5 which is carried out to study the effects of variation of physical parameters such as number of vanes, vane angles, vane height, vane width, on axial volumetric flow rate profiles of similar heated plate length scale (radius R).After selecting the geometry the effects of temperature differences were observed and discussed, followed by the geometric scaling study in which a scaling factor S is used to study the variation in the axial volumetric flow rate. Final chapter includes the concluding discussion with some suggestions for the future work which follows the references. Appendices B to D include the dictionaries that were used for the OpenFOAM solver, while Appendix A is about two other alternative meshing methods for reference.

CHAPTER 2

2. BACKGROUND AND PREVIOUS WORK

2.1. Background research

2.1.1. Theoretical modeling of dust devils

Several attempts have been made in previous years to model the naturally occurring dust-devils. These models are enlightening and worth reviewing prior to any attempts of assessments of energy extraction possibilities from the potential that is present in this type of the flow. These studies can be used as bench mark studies for the validation of the numerical modeling of experimental setups or environmental conditions that are used to create columnar vortices similar to dust devils as it is done in the related studies [1] [15] [20] . One of these models is based on the assumption that dust devils can be modeled as heat engines. This model by Renno et al. [7] can be used to estimate the axial and tangential velocity profiles with-in a dust devil vortex. The distribution of axial velocity w is assumed uniform across the vortex core and it decays exponentially outside. The axial velocity is a function of sensible heat flux (F_{in}) into the air, the temperature difference (η) between convective layer and the surface, the co-efficient of viscous dissipation(μ) in the atmosphere and the atmosphere`s ability to cool the air in the convective layer by radiation ($8\varepsilon\sigma T_c^3$).

$$w \approx \left[\left(\frac{C_p}{8\varepsilon\sigma T_c^3}\right)\frac{\eta F_{in}}{\mu}\right]^{1/2} \tag{2-1}$$

The model estimates the maximum tangential velocity component as a function of universal gas constant, R, the surface mean temperature, T_s , the fraction of mechanical energy lost due to viscous effects at the surface γ, the horizontal thermal efficiency η_H and $X = \frac{C_p}{R}$

$$v = \left\{R\overline{T_s}\left[1 - exp\left(-\frac{\gamma\eta}{\gamma\eta - 1}\right)\left(\frac{1}{X}\right)(\eta_H)\right]\right\}^{1/2} \tag{2-2}$$

Gu Zhaolin et al. [20] used Renno et al. [7] model for the estimation of velocity fields and compared them with the simulated results. Gu Zhaolin et al. found that most values of the

maximum tangential velocity in the simulated modeled dust devils were close to the range predicted by Renno et al. [9].

Apart from the above scalable model of dust-devils several authors relate cross-sectional radii of dust devils to the tangential velocity distribution. Tangential velocity has a maximum value at the radius of the core, and the region of maximum vertical velocity often corresponds to the area where the thermal updraft is a maximum, which is in the center of the core. The maximum vertical velocities coincide with the region of lowest pressure, or where the horizontal pressure gradient is the greatest at the surface. Because of these features of the velocity distribution, Rankine vortex model [8] is often used to make a comparison with field observations, laboratory and numerical simulations of dust devils [1] [23] [24] [25] [26] [15]. The conditions for a Rankine vortex model are assumed to be steady state, two dimensional (no variation in the z direction) and the radial and vertical velocities are assumed to be zero. The Rankine vortex model is a combination of solutions for a solid body rotation inside a vortex core and a potential vortex outside the core as it is shown in equation (2-3). The radius of the vortex core and the radius of maximum tangential velocity is r_c.

$$V_\theta = \frac{\Gamma_\infty r}{{r_c}^2} \; when \; r < r_c \, , \; V_\theta = \frac{\Gamma_\infty}{r} \; when \, r > r_c \tag{2-3}$$

Another theoretical vortex model is the Burgers-Rott vortex solution [9] [10] which is also used to make a comparison with the numerical simulations of dust devils. Burger`s model, unlike Rankine`s model, gives a continuous representation of tangential velocity. Burger`s model assumes a linear variation of radial velocity with the radius, thus it implies that axial velocity must not vary with radius and stay linear with height to conform with the continuity equation

$$V_r = -\frac{a}{2} r \tag{2-4}$$

$$V_\theta = \frac{\Gamma_\infty}{2\pi r}\left\{1 - exp\left(-\frac{a r^2}{4v}\right)\right\} \tag{2-5}$$

$$V_Z = \; az \tag{2-6}$$

Above Eqns. (2-4) (2-5) (2-6) show the radial, tangential and vertical velocities in the Burgers-Rott [9] [10] vortex model, where V_r, V_θ and V_Z are radial, tangential and vertical velocities respectively; Γ_∞ is the circulation at a distance far away from the vortex core; r is the radial, z is the vertical position, v is the kinematic viscosity and a (m^{-1}) is a constant.

Another vortex model used in dust-devil analysis is the Lamp-Oseen vortex model. This model is also a continuous model like the Burgers-Rott. This model consists of two iterative constants C_1 and C_2 which can be iteratively found to fit any tangential velocity profile of dust-devil or dust devil like vortex [21] [22] [14].

$$V_\theta = \frac{C_1}{2\pi r}\{1 - exp(-C_2 r^2)\} \tag{2-7}$$

These theoretical vortex models are not accurately applicable to the case studied in this document but they have been used for the comparison with the simulated results in various studies related to dust devils. Kanak [15] used Burger-Rott and Rankine vortex models to make a comparison with the simulated tangential velocities. Sinclair [1] compared the dust devil measurements with a Rankine vortex as it is shown in Figure 2.1. Greely [14] used the Lamp-Oseen model for the laboratory experiments in ASUSVG, where cyclostrophic balance was assumed and the data from pressure transducers was used to fit the curve of tangential velocity by iterating the constants C_1 and C_2 in equation $(2\text{-}7)$ of Lamp-Oseen vortex model.

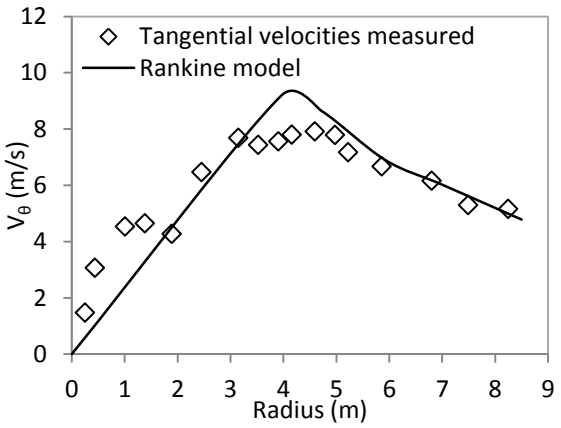

Figure 2.1 Tangential velocity profile measured by Sinclair, with Rankine vortex model

A simpler model for concentrated vortices was proposed by Vatistas et al. [16], which fits well with the observations of tangential velocity. Other velocity components are derived from the equations of motion.

$$\overline{V_\theta} = \frac{\bar{r}}{(1 + \bar{r}^{\,an})^{1/n}} \tag{2-8}$$

Where, $\overline{V_\theta} = \frac{2\,\pi V_\theta r_c}{\Gamma_\infty}$, $\bar{r} = \frac{r}{r_c}$, $a=2$ and n are general constants. Based on experimental observations it was assumed that tangential velocity component does not depend strongly on axial direction. These assumptions lead to following equation for radial velocity.

$$\overline{V_r} = \frac{2(1+n)r^{-2n-1}}{1 + r^{-2n}} \tag{2-9}$$

Where $\overline{V_r} = \frac{V_r r_c}{v}$, equation (2-9) and continuity equation lead to following equation for axial velocity

$$\frac{\overline{V_z}}{\bar{Z}} = \frac{4n(1+n)r^{-2n+2}}{(1 + r^{-2n})^2} \tag{2-10}$$

where, $\overline{V_z} = \frac{V_z r_c}{v}$ and $\bar{z} = \frac{z}{r_c}$ and distributions with n less than one should not be used, due to the presence of singularities at the center in equation (2-9) and equation (2-10)

2.1.2. Natural convection over horizontal plate

Usually the laboratory setups developed to mimic the naturally occurring vortices have two essential capabilities, one of those capabilities is to be able to generate an updraft and the other is to apply swirl to the upward flow. As it was discussed in prior sections, there are several studies in the literature where natural convection over a flat horizontal surface [6] [4] [20] [15] is utilized to produce an updraft to generate vortices. This section therefore is present for a brief insight in the area of natural convection over horizontal plates. In general, natural convection is caused by the buoyancy force that arises from density differences, which are generated by temperature gradients within a fluid. In practical applications of natural convection, the extent of the heat transfer is usually estimated by

experimentally developed Nusselt number correlations. These co-relations are usually in the following form.

$$Nu = C(Gr\ Pr)^m \tag{2-11}$$

Where, Gr is the Grashof number $\frac{\beta g\, \Delta T L^3}{\upsilon^2}$ and Pr is the Prantl number $\frac{\mu Cp}{k}$,C and m are correlation constants. These correlations have limited applicability for heated horizontal plates, since they are limited to certain range of Rayleigh numbers which is usually not more than 10^{11} [37]. Yousef et al. summarized the data and correlations used in free convection from horizontal rectangular surfaces heated and facing upward with a range of Rayleigh numbers from 2×10^5 to $3\,x\,10^{10}$. Kobus et al. [36] presented a dimensionless correlation for the heat transfer from horizontal isothermal circular disks for Rayleigh number from 3×10^2 to 3×10^7. These studies show that experimental studies in the literature typically tackle heat transfer characteristics of horizontal upward facing heated plate.

Apart from heat transfer related studies, various studies investigated flow characteristics of natural convection over a horizontal surface. These studies showed that at low Rayleigh numbers the flow results in the formation of a convective plume at the center that develops as a result of an inward flow towards the center of the plate [32] [33] This convective plume is necessary for the formation of convective vortices in experimental setups which utilize natural convection as a source of updraft. When the Rayleigh number is increased further, flow starts transitioning towards turbulence and starts separating from the horizontal surface at locations close to the edges, resulting in a non-cellular flow. Another study [34] based on natural convection over horizontally heated plates, with a wider range of Ra numbers (10^6 to 10^{15}) and hence wider length scales, defines the flow types from the edge to the center of a heated plate as follows:

- laminar boundary layer near the leading edges,
- transitional flows which are characterized by three dimensional separations
- by attachment of the low-temperature fluid into the surface downstream of the separation,
- fully turbulent flows and colliding flows near the centerline of the plates.

Simpson et al. [12] showed that a nucleating protrusion can be added at the center of the heated plate to support the formation of the plume. After the formation of the central plume the swirl can be imparted via azimuthal addition of guided vanes to tangentially direct the flow towards the plume. Present study includes the discussion of the effects of the geometrical parameters such as vane width, vane height and number of vanes on the axial volumetric flow rate at the center, and hence the strength of the plume without the presence of any nucleating protrusion.

2.1.3. Models utilizing heated surface to study columnar vortices

A study performed by Fitzjarrald [11] involved a laboratory apparatus capable of mimicking the naturally occurring dust devils, which was constructed considering the simplest boundary conditions. It consisted of a circular, uniformly heated aluminum plate and 20 Plexiglas vertical windows (vanes) around the circumference to impart tangential velocity component to the incoming air. The test chamber, inside the vanes and above the heated plate, was scaled in order to be compared with the field data and applicable theories of dust devils. Only two controlling parameters were present in the experiment; plate temperature and the angle of inlet windows.

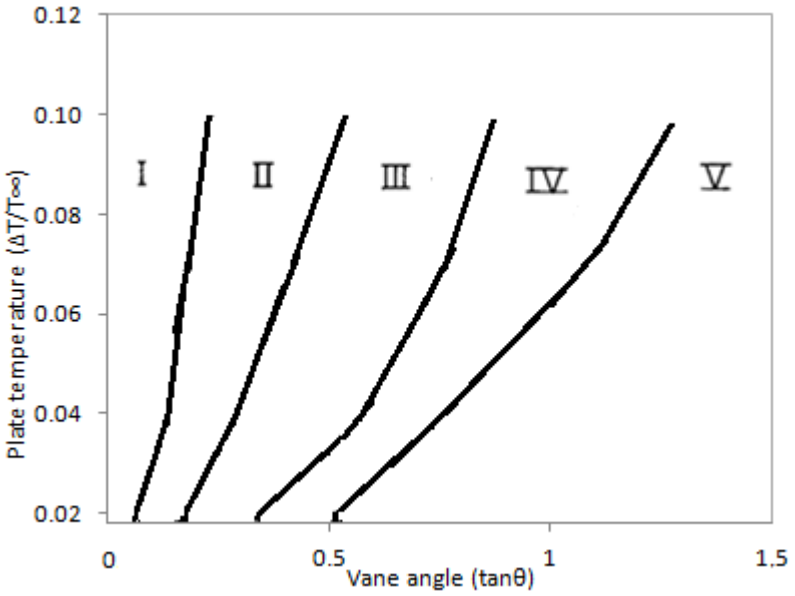

Figure 2.2 Observed vortex types vs. plate temperature and inlet angle, showing the dependence of observed vortex characteristics on experimental conditions

The plate temperature determines the buoyant acceleration and the angle of inlet windows determines the angle of the streamlines at the inlet i.e. swirling. The length scale is the radius of the heated plate whereas the velocity scale is the convective velocity. The results were presented using a stability parameter consisting of both independent parameters. Using different plate temperatures and vane angles, different flow patterns were observed. The investigations of Fitzjarrald, D.E included the relationship between vane angle, plate temperature (i.e. stability parameter) and the type of the flow. This stability parameter does not include the radial length scale i.e. radius of heated plate, which makes its applicability limited to that particular length scale. Fitzjarrald [11] observed five different types of flows based on temperature differences and vane angles as shown in Figure 2.2.

The flow type-I is obtained when the induced swirl is small i.e. vane angles are higher and it showed no significant vortex, the flow type-II is obtained by increasing the swirl a bit more than flow type-I, and it showed a one cell, small, laminar and more persistent vortex. By increasing the swirl a bit more than the flow type-II, the flow type-III was obtained, which consisted of a two-cell motion, a vortex of stronger circulation but with an oscillating vortex breakdown, which is observed as a stagnation point along the center line of the flow accompanied by turbulence. When the swirl was increased more or the plate temperature was decreased different flow type conditions were obtained named as type-IV flow, in which the vortex breakdown location stays close to the surface but with more turbulent features. Core radius increases with height at a higher rate than was observed in flow type-IV. The flow type V results when buoyancy caused by the heated plate is not enough to overcome rotation. The swirling flow is spread over the test chamber.

Another example of simulation of generation of thermally driven vortices is a numerical study by R.K Smith and Leslie [4]. The physical conditions used in the numerical model were a circular heated plate at the center surrounded by unheated floor with no slip condition. Swirl is generated by a rotating porous screen. This study is similar with current study in the sense that it is also a computational or numerical model of a thermally driven laboratory vortex generator. Boussinesq approximation was used to account for density effects. The main non-dimensional parameters used in this study were a pseudo-Rayleigh number and a swirl parameter.

$$Ra = g\frac{\Delta T}{T_e}\frac{{R_s}^3}{KM^2} \tag{2-12}$$

$$Rt = \frac{Ve\ R}{R_s}\left[g\frac{\Delta T}{T_e}R_s\right]^{-1/2} \tag{2-13}$$

where R_s is the radius of the heated plate, R is the radius of rotation, Ve is the velocity of rotation T_e is the ambient temperature, ΔT is the difference of temperature between heated plate and the ambient. Swirl parameter was used as a measure of rotational constraint for a given level of thermal forcing. The numerical simulation corroborated well with the experimental results of Fitzjarrald [11] and provided a demonstration of main features of dust devils as observed by Sinclair. These numerical simulations showed how rotationally induced pressure gradients can supplement buoyancy forces in accelerating the vertical flow in dust devils to account for large vertical accelerations that cannot be just because of buoyancy forces.

Kanak et al. [15] performed large eddy simulation of convective boundary layer using a 35 m horizontal spacing grid and found the existence of vertical vortices in the convective boundary layer. This model was capable of simulating the initiation of weak vertical vortices. In Kanak's recent work (2005) [38], a 2-m grid spacing large eddy simulation of the convective boundary layer was performed in order to examine the physical characteristics of dust-devil-scale vortices. This model having results that were in good agreement with the general features of the dust devils, was limited in a number of aspects, such as the pressure drop inside the simulated vortex core was not as huge as expected, and the simulated vortex wind speeds were less than $10\ m\ s^{-1}$. It was proposed that initial conditions of the simulation might have an important effect on the creation of vertical vortices.

Zhaolin et al. [20] conducted dust devil-scale large eddy simulations, with the introduction of boundary conditions as ground temperature, initial vortex and surface momentum impact height. After matching these boundary conditions with Sinclair's field measurement, the simulation was validated using the maximum tangential velocity, updraft velocity and pressure-drop in the inner core region and found in good agreement. The major finding was the development of severe dust devils, even for smaller temperature differences or weaker

buoyancy, if provided with strong incipient vortices. These studies demonstrate the ability of numerical models to capture the characteristic features of dust devil scale vortices.

2.1.4. Experiments for power production

Experimental lab-based buoyancy-induced vortex facility developed by Simpson et al. [12] consisted of Ground heating of $1\ m\ x\ 1\ m$ with a controlled heater of $4.8kW$ power, with 12 planar aluminum vanes of $0.35\ m\ x\ 0.6\ m$ dimensions. The heated surface was made of aluminum with $1m\ x\ 1m$ dimensions. The outcomes of this experiment in lab were a vortex of up to $4m$ height, with surface core diameter of $5 - 25cm$. The temperature of the center line of the vortex at $5mm$ above the surface was found to be $46°C$ which was comparable to desert air temperatures $2m$ above surface.

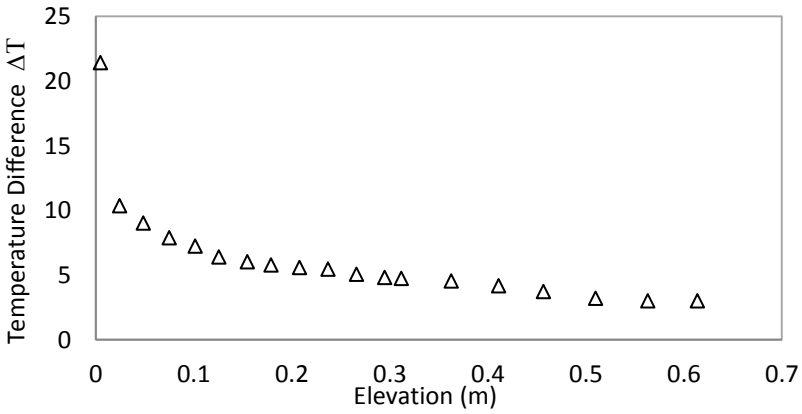

Figure 2.3 Measured temperature profile along the Vortex centerline for the field Vortex

Simpson's et al. [12] compared the circulation distribution at an elevation of 0.2 R for a plate temperature of $100°C$ with that of a natural vortex and it was found in good agreement. The circulation distributions $\Gamma_{(r)}$ are normalized by the maximum circulation Γ_m. The characteristic radius of the vortex (r_c) is selected at the region where the circulation becomes radially-invariant. The radial distance is normalized by the characteristic radius, Figure 2.4 shows the corresponding radial distributions of the circulation $\Gamma_{(r)}/\Gamma_m$

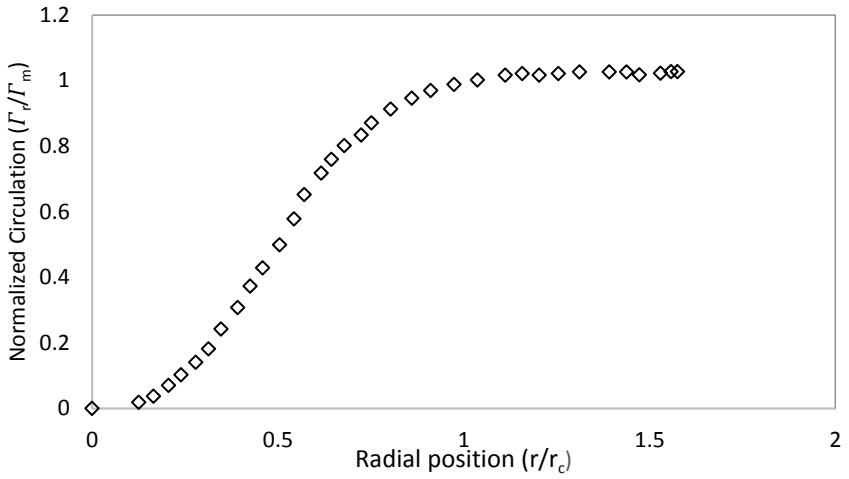

Figure 2.4 Variation of normalized circulation with the radial position [12]

Another outdoor meter-scale setup is also present in the study of Simpson et al. [12]. This setup contains 12 radially installed vanes of height $0.6\ m$ and width $0.4\ m$. The angles of the vanes were adjustable. In this particular experiment the angle was set equal to $30°$. The vanes were installed on a heated surface of $1\ m$ diameter. The boundary conditions of the experiment were described as follows. Ambient temperature was in between $31 - 34\ °C$. The surface temperature of the centrally located hotspot on the heated surface was found as $55°C$. The floor temperature around the heated surface was equal to $40°C$. Figure 2.3 shows the measured vertical temperature distributions at the center of the field vortex [12]. This graph is used to verify the results of the simulation.

2.1.5. Swirling flows

Apart from similarities with dust-devils, the type of the flow that this experimental setup can be classified as a swirling vortex. A flow with spiral motion in tangential direction along with axial and radial directions is regarded as a swirling flow [29]. This type of flow improves flame stability if introduced in a combustion chamber, by forming a toroidal recirculation zone. Several other advantages, including the introduction of swirling motion to the jet flow can lead to a higher ambient entrainment flow and enhance flow mixing [29]. The parameter that could be used to characterize the swirl strength of a swirling flow leads to several options. Some researchers suggest the use of vane angle directly [31]. Another widely used parameter is the swirl number. Swirl number was originally proposed by

Chigier and Beer [30], which is the ratio of axial flux of angular momentum to the axial flux of axial momentum. A modified form of swirl number S is defined in equation (2-14)

$$S_w = \frac{\int_0^R V_z V_\theta r^2 \, dr}{R \int_0^R {V_z}^2 r \, dr} \tag{2-14}$$

where V_z is the axial and V_θ is the tangential velocities, and R is the hydraulic radius. H.J Sheen et al. [29] studied the relation between the angle of guided vanes and the swirl number under various flow conditions. H.J Sheen found that the modified swirl number depends on both the vane angle but also the Reynolds number. This shows that modified swirl number can be used to characterize the swirling flows and this can be applied to the case discussed in this document.

2.1.6. Summary of the chapter

The power generation potential present in dust devil scale vortices can be tapped by developing an apparatus that could deliberately form similar atmospheric vortices. Studies are present in the literature discussing the field measurements and observations regarding the structure of naturally occurring dust devils [1][2][3].These studies provided a bench mark validation for the later studies, some of which discuss the mechanisms of naturally occurring dust devils through simulations of natural physical environment with pre-decided boundary conditions[20][15]. Some studies include the use of experimental lab apparatus capable of mimicking the features present in dust devil scale vortices [11] [12] [13]. Present study is focused on the investigations based on numerical simulations of the meter scale experimental setup that can produce vortices similar to dust devils, using OpenFOAM, open source computational fluid dynamics software. The next chapter is about the description of the methodology used to develop the numerical model.

CHAPTER 3

3. METHODOLOGY

The present study involves numerical simulations based on finite volume method using OpenFOAM, open-source computational fluid dynamics software [40]. This chapter describes the research methodology, which consists of (i) physical and geometrical parameters influencing flow, (ii) governing equations, (iii) mesh characteristics and boundary conditions, (iv) numerical method and the solver used in this study and (v) post processing methodology and parameters. Furthermore, results, related to grid convergence and verification of boundary conditions are also presented.

3.1. General description of the physical model

Basic flow geometry is shown in Figure 3.1, which consists of a circular heated plate at elevated temperature surrounded by an unheated floor. Both the heated plate and floor are open to atmosphere. Circular heated plate is surrounded by a number of vertical thin flat plates, referred to vanes throughout the thesis. Vertical vanes are considered as the core focus of this thesis as they guide the entrained flow away from the center of the plate to induce circulation. The influence of vane width, c, vane height, h, and vane angle, θ, and plate radius, R, on the flow field will be investigated to characterize the setup illustrated in Figure 3.1 .

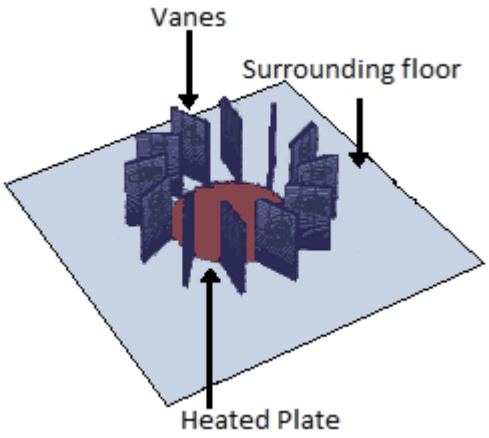

Figure 3.1 An oblique sketch of the experimental setup showing major components

Vane angle can be defined as the angle between the vane and an imaginary radial line stretched from the center of heated surface as shown in Figure 3.2. Vane angles can be positive and negative, which would only influence the direction of circulation. Vane width is defined as the horizontal length of the vanes whereas vane height is the distance from the floor to the top of the vane. Vanes and the heated surface are open to atmosphere. The effects of vane thickness are neglected for simplicity in this study.

3.2. Governing equations

In free convection problems, the driving force of the flow is the density difference that occurs because of temperature variation. The flow field is considered to be incompressible and the buoyancy effects are considered through Boussinesq approximation, which accounts for density variation based on temperature only. The governing equations for incompressible fluid flow including the Boussinesq approximation are given as follows:

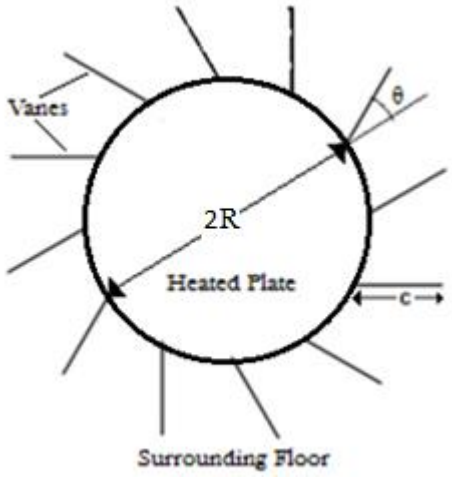

Figure 3.2 Top view of the basic flow field, heated plate with vanes

$$\nabla \mathbf{u} = 0 \tag{3-1}$$

$$\rho_o \left(\frac{\partial \mathbf{u}}{\partial t} + (\mathbf{u} \cdot \nabla)\mathbf{u}\right) = -\nabla p + \mu \nabla^2 \mathbf{u} + \rho_o (1 - \beta \Delta T)\mathbf{g} \tag{3-2}$$

Where the density of ambient air is ρ_o, $\mathbf{u}$ is the velocity vector, p is the pressure and β is the expansion coefficient which can be approximated as $1/T$ for ideal gases.

The scalar transport-diffusion equation for the temperature is given as follows:

$$\frac{\partial T}{\partial t} + (\mathbf{u} \cdot \nabla) T = \alpha \nabla^2 T + \phi \tag{3-3}$$

Where T is the temperature, α is the thermal diffusivity, and ϕ represents a source term.

3.3. Numerical method, computational domain and boundary conditions

Equations (3-1) (3-2) (3-3) are solved using the tools provided by OpenFOAM, leading open-source computational fluid dynamics (CFD) software, which consists of a set of C++ libraries using finite volume method to solve partial differential equations on the Linux platform [39]. OpenFOAM also offers precompiled solvers each designed for frequently used equation sets, including compressible and incompressible Navier-Stokes equations representing fluid flow [40]. The solver used in this study is a pressure based method for incompressible transient flows which includes Boussinesq approximation as given in equations.(3-1) (3-2) (3-3).

Specifically, the numerical method of the solver is a combined PISO (Pressure implicit with splitting operators) - SIMPLE (semi-implicit pressure linked equations) for transient simulations allowing large time steps [41]. The solver allows using variable time step based on Courant–Friedrichs–Lewy (CFL) condition, in which every time step is selected such as to keep Courant number lower than 0.5 for all simulations. Courant–Friedrichs–Lewy (CFL) condition is one of the necessary conditions that are required for the convergence of the solution. Discretization schemes and the interpolation scheme used for energy equation, momentum and continuity equation are given in the Table 3.1

Table 3.1 Discretization scheme as used in OpenFOAM.

Discretization	**Scheme**	**Interpolation**
Time	Implicit	Euler
Gradient	Gauss	Linear
Divergence	Gauss	linear / upwind
Laplacian	Gauss	Gauss linear uncorrected

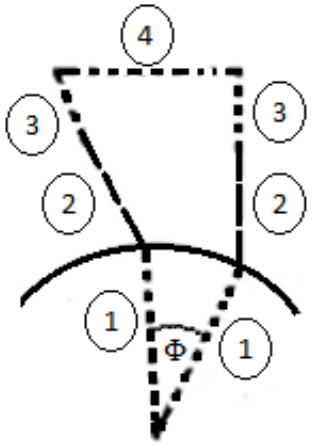

Figure 3.3 Top view of the flow domain and boundary conditions

The thermo-physical model used in the solver is a pressure temperature system from which other properties are calculated using an ideal gas model defined by fluids molecular mass, M,

and constant specific heat, c_p [40]. Transport properties such as dynamic viscosity,μ, and thermal diffusivity, α, are computed using constant values for fluid's kinematic viscosity, $\nu = \mu/\rho$, and Prandtl number, $Pr = \nu/\alpha$.

As the flow between the vanes is repetitive along the angular direction, the flow domain, as illustrated in Figure 3.3, is selected considering a sector of the whole geometry to minimize the computation time and post processing data handling. This results in a truncated circular plate in shape of a piece of pie with a span characterized by a central angle of ϕ. The value of angle ϕ depends on the number of vanes attached to the heated plate as it can be seen in the Figure 3.3, that vanes put a limit to the value of ϕ .Sector's vertical internal surfaces those exposed to flow, as shown with labels 1 and 3 in Figure 3.3, are modeled using cyclic boundary condition for all transport variables. Surface representing vertical vanes are labeled with 2, where no-slip boundary condition is imposed for velocity and constant temperature for the energy equation. At circumference at a further distance, surface marker with label 4 and top surface is defined by following conditions. The boundary condition for temperature switches between the given constant value and zero-gradient depending on the direction of the velocity. The boundary condition for the velocity is same for top surface i.e. it switches between a constant value and zero gradient depending on the direction of the velocity but it is different for the surface 4.The boundary condition for velocity for surface 4 is defined as follows; when pressure is known at inlet, velocity is evaluated from the flux normal to the patch, also it switches between fixed value and zero gradient depending on direction of velocity. All values for pressure at boundaries are calculated by the solver.

The whole bottom surface is considered with no-slip velocity boundary condition while the heated plate covering a radial distance from the center to the vanes (between 1-1) is considered at an elevated temperature than the remaining part (between 2-2 and 3-3) of the bottom surface. Heated plate is the only surface at an elevated temperature, whereas all other solid surfaces and internal field is given an initial value that is equal to the ambient temperature. Simulations are initialized with zero velocity field and ambient temperature and carried out until steady state is reached which is decided by tracking the variation of two independent points in time .When the variation of two independent points becomes negligible steady state is considered to be achieved.

3.4. The turbulence model-RAS

Reynolds-averaged stress (RAS) turbulence model is used to solve for the mean turbulence behavior of the flow. The model used in this study is standard $k-\varepsilon$. The initial values for the model are calculated using the following expressions.

$$k = \frac{3}{2}(UI)^2 \tag{3-4}$$

Where I is the initial turbulence intensity [%] which is calculated as $0.16\,Re^{-1/8}$, where Re is the Reynolds number. U is the initial velocity magnitude.

$$\varepsilon = C_\mu^{3/4} k^{3/2} l^{-1} \tag{3-5}$$

Where l is the turbulence of eddy length scale, which is calculated by $l = 0.07L$,where L is the characteristic length which in this case is radius . C_μ is a $k-\varepsilon$ model parameter whose value is typically given as 0.09

3.5. The computational grid

Structural grids based on mostly hexahedra cells with prisms at the center, are generated for each case. These cases are represented by geometric parameters such as vane width, c , vane height, h, and vane angle, θ, and plate radius, R and vane spacing ϕ. Each grid consists of six blocks, with three lowers blocks for regions between labels 1-1, labels 2-2 and labels 2-2 of Figure 3.3 and three upper blocks attached to the top of lower blocks. This setting makes it possible to use mesh refinement in regions where it is necessary and avoid it when it is not necessary, to save computation time.

Table 3.2 Refinement of different blocks of the mesh

Block	Angular Refinement	Radial Refinement	Vertical Refinement
11	Medium	Fine	Fine with grading from Heated Plate
22	Medium	Medium	Fine with grading from floor
33	Medium	Medium	Fine with grading from floor

11`	Medium	Fine	Coarse
22`	Medium	Medium	Coarse
33`	Medium	Medium	Coarse

The resulted mesh is a cyclic mesh with grid resolution that can be represented in angular, radial and vertical directions for each block as shown in Table 3.2 .The angular resolution of the whole mesh is necessary to be the same, whereas, there are other restrictions as well such as radial resolution must be same for every pair of upper and lower blocks, vertical resolution of all lower blocks and all upper blocks must be same. The appropriate resolutions were decided later on after the grid convergence study and validation from experimental results.

3.6. Verification

The verification of rotational symmetry, applicability of cyclic boundary condition, selection of sector`s span and as well as the check on grid quality at the center of the mesh is done through a simplified problem in the case of heated plate without vertical vanes.

3.6.1. Selecting span of the representative sector

Solution obtained through a full circular plate are compared with the solutions obtained through sectors with spans of $\phi = 18^{\circ}, 30^{\circ}, 42^{\circ}, 60^{\circ}$ and 360°. All domains are meshed with similar cell spacing to ensure that results are independent of discretization errors. The grid resolution is described in terms of cell spacing for all cases as follows; 1.2° cell spacing in angular direction, $0.032\,m$ in vertical direction and $0.04\,m$ in radial direction. The heated plate was kept at $314\,K$, while the surrounding floor was kept at $307\,K$.

Table 3.3 Root mean square error for different spans

Angular span (ø)	R.M.S.E
18 ˚	8,16E-06
30 ˚	5,66E-06
42 ˚	6,15E-06
60 ˚	2,45E-06

Table 3.3 contains the root mean square errors for different angular widths with respect to the 360° mesh, illustrating that assumption of rotational symmetry is valid and it is a cyclic flow field as all cases considered are independent of the sector span and compatible with full-circular plate results.

3.6.2. Grid convergence study

A grid convergence study is performed on this grid to evaluate the overall order of accuracy of the solver and to determine reasonable grid resolution. The grid convergence study is again carried out without placing the vanes. A series of simulations was performed on an angular span of $\Phi = 30^{\circ}$, with varying grid sizes from $9k$ to $86k$ number of cells. The $86k$ cell grid was taken as reference grid and the root mean square error, RMSE, is calculated and plotted with all the grid sizes with respect to the 86k cell grid. It was found that with $9k$ grid size the discretization error was highest and it started decreasing with the increase of refinement of the grid. Slope in Figure 3.4 represents the overall order of accuracy of the solver, which is found to be less than second order accuracy.

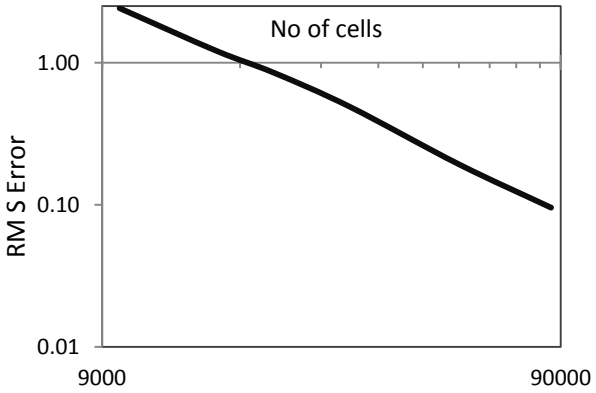

Figure 3.4 Variation of logarithmic root mean square error with respect to the grid resolution

3.7. Post processing

Post-processing is done using an open source postprocessor Paraview. In general the focus of post-processing is velocity fields in radial angular and vertical directions and temperature fields. Several parameters of swirling flows, like circulation, angular velocities and axial

volumetric flow rate are evaluated as a means of characterization of the flow field. Circulation is measured using the tangential velocity component for various radial positions, using following equation (3-6),

$$\Gamma_r = \int_0^{2\pi} V_\theta \, r \, d\theta \tag{3-6}$$

Where Γ_r is the value of circulation at the radial position r and V_θ is the tangential velocity at that radial position.

Another useful parameter is the axial volumetric flow rate, as shown in equation (3-7) which can provide information about vortex stability, distinguish regions of radial inflow, stability and decay of the vortex in the axial direction.

$$V_f = \int_0^{2\pi} \int_0^{r} V_z \, r \, d\theta \, dr \tag{3-7}$$

Where V_f is the axial volumetric flow rate, V_z is the vertical velocity at radial and angular position corresponding to r and θ.

A parameter derived from the axial volumetric flow rate is the average axial velocity as shown in equation (3-8) that can be obtained by dividing V_f by the cross sectional flow area above the heated plate within the vanes

$$V_a = V_f / A_f \tag{3-8}$$

The peak of the average axial velocity is represented as V_{pa} and is obtained by looking at the peak value of average vertical velocity which is also used to compare different flow conditions.

Another useful parameter is the swirl number S_w as described in equation (2-14) which will be used to quantify the swirl intensity of the flow, that is induced by the vane angles.

The velocity scale used in this study is simply the convective velocity described as below [11].

$$V_c = \sqrt{g\beta\Delta TR} \tag{3-9}$$

Axial volumetric flow rate is scaled by the following relation

$$V_{fc} = \pi R^2\sqrt{g\beta\Delta TR} \tag{3-10}$$

Elevations and radial positions are simply normalized by respective vane heights h and heated plate radius R.

3.8. Summary of the chapter

Current study is based on the numerical modeling of an existing meter scale experimental setup. The numerical model was developed using OpenFOAM. A simplified grid was developed by applying cyclic boundary condition to reduce the computational time, memory space and post processing time. After the selection of the grid style, grid refinement strategy was developed to avoid unnecessary grid refinement in regions which are not focused on this study. The transient solver used in this study assumes incompressible flow and density variations were accounted using boussinesq`s approximation. Thermo-physical properties were modeled using a pressure temperature system from which other properties are calculated using an ideal gas model defined by fluids molecular mass, M, and constant specific heat, c_p [40]. Transport properties such as dynamic viscosity μ and thermal diffusivity α are computed using constant values for fluid's kinematic viscosity $\nu = \mu/\rho$, and Prandtl number $= \nu/\alpha$. Turbulence modeling was based on standard $k - \varepsilon$ model. A grid convergence study was performed to check the order of accuracy in terms of discretization errors. The next chapter is about the discussion of the validation studies of the numerical model.

CHAPTER 4

4. MODEL VALIDATION AND FLOW FIELD DESCRIPTION

4.1. Validation studies

This section starts with a brief description of the general physical and geometrical parameters and flow field that is obtained by simulating the experimental setup. This follows the discussion about validation studies, based on theoretical vortex models and previous experiments. Validation studies were performed to assess the capabilities of the solver and the mesh.

4.2. General flow field description

The results of the simulations of the columnar vortex included the thermal and velocity fields, showing the warm and low pressure core, radial inflow at the bottom and subsequent rotation and rising of the air within and around the vortex core. General physical parameters that were used for the validation studies of the simulations based on the experiments of Simpsons et al. are described in Table 4.1.

Table 4.1 General physical and geometrical parameters, which are used in validation studies

Working fluid	$\boldsymbol{Air}$
Radius of the heated plate ($\boldsymbol{R}$)	$0.5\ m$
Height of the vanes (h)	$0.6\ m$
Width of the vanes ($\boldsymbol{c}$)	$0.4\ m$
Angular width ($\boldsymbol{\Phi}$)	30°
Angle of vanes ($\boldsymbol{\theta}$)	$15^{\circ} - 55^{\circ}$
Number of vanes	12
Overall range of dimensions	$3m\ x\ 3m\ x\ 3m$

The numerical simulation was able to capture the formation of a stationary, anchored columnar vortex, as it can be seen in Figure 4.1 which shows the stream lines of a columnar vortex formed when physical conditions of Table 4.1 were simulated with a vane angle of 30° and a temperature difference of 22°C between the isothermal heated plate and the ambient. The streamlines show radial inflow at the bottom region which starts rotating and rising while moving towards the center.

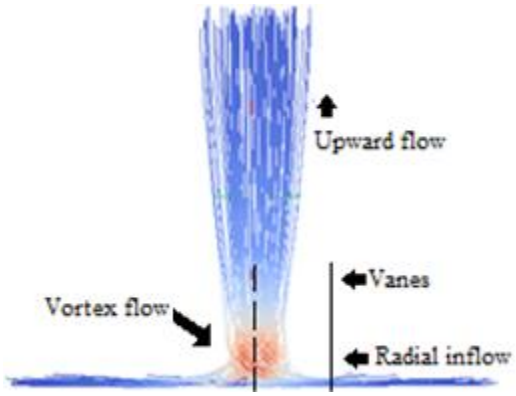

Figure 4.1 Streamlines of the flow, showing the formation of vortex at the center for a vane angle of 30° and plate ambient temperature difference of 22 °C

In order to see a complete picture, axial volumetric flow rates as described in equation (3-7) were plotted in Figure 4.2 for this case, to observe and extend the understanding of the flow field. The axial volumetric flow rate first rises from the bottom which indicates the radial inflow region, after reaching the peak the axial volumetric flow rate stays constant and then starts decaying again. The region of the constant flow rate in this plot reflects the stability of the vortex.

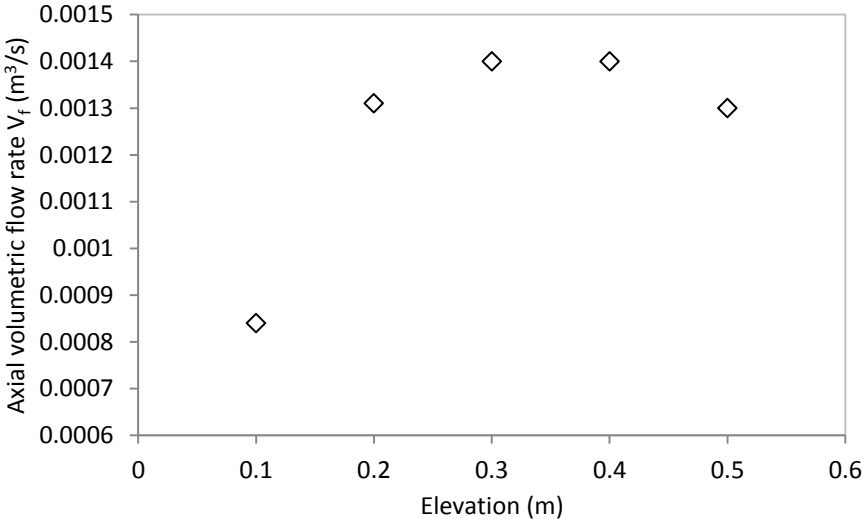

Figure 4.2 Variation of axial volumetric flow rate with elevation

4.3. Validation studies based on theoretical vortex models

Based on the discussion about Figure 4.2 , the stability region of the plot starts at an elevation of 0.6 R. So in order to verify the formation of a vortex tangential velocities at the elevation of 0.6R of simulated vortex model based on the same geometry as defined in Table 4.1 with a vane angle of 30˚ and a temperature difference of $\Delta T = 22^{\circ}C$ between heated plate and the ambient were plotted in Figure 4.3 against the theoretical vortex models such as Rankine vortex model, and Burgers vortex model as described in equations (2-3), (2-5). An empirical vortex model for concentrated vortices as proposed by Vistas et al. as described in equation (2-8) is also included in Figure 4.3 which gets the best fit for the case in hand for a value of n =1.2. This proves that a vortex is formed at the center region and it is similar with dust devil vortices, as these models have been extensively used by several authors to study dust devils. The resemblance of the flow in this experimental setup with dust devil vortices supports the proposition that if up-scaled this model can produce flows similar in magnitude with the dust devils.

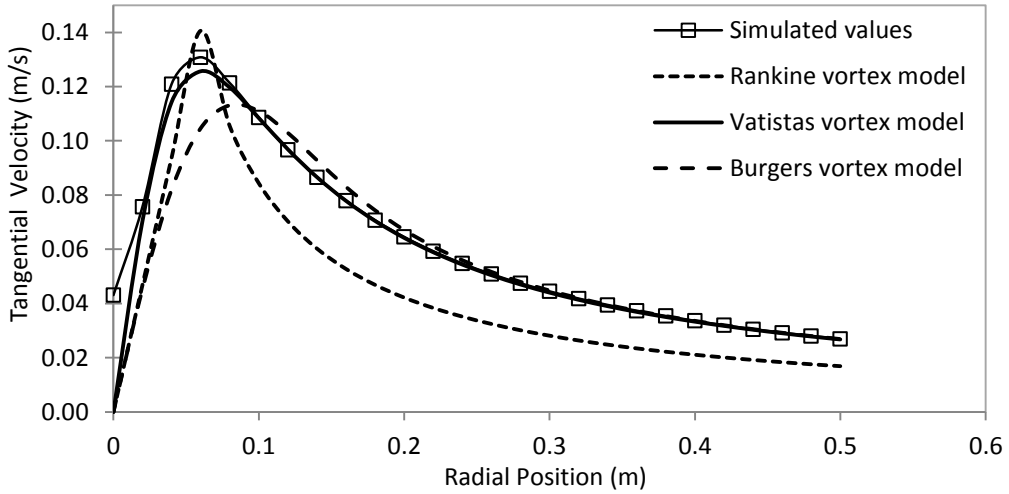

Figure 4.3 Comparison of tangential velocities of simulated vortex with theoretical vortex models at an elevation of 0.6R

4.4. Validation studies based on experimental results

A validation study was also carried out, against the experimental results of Simpsons et al. for this cyclic grid having the physical features as described in Table 4.1. An important feature of the flow as described by Simpsons et al. [12] is the centerline temperature profile. This temperature difference is a necessary condition for the vortex to form. The experimental centerline temperature profile as obtained by Simpsons et al. [12] for a vane angle of 30˚ and ΔT of 22˚C is plotted against the simulated centerline temperature profile in Figure 4.4. In Figure 4.4 vertical axis shows the temperature difference between the center of the vortex at a particular elevation and the ambient, whereas horizontal axis shows the elevation from the heated plate.

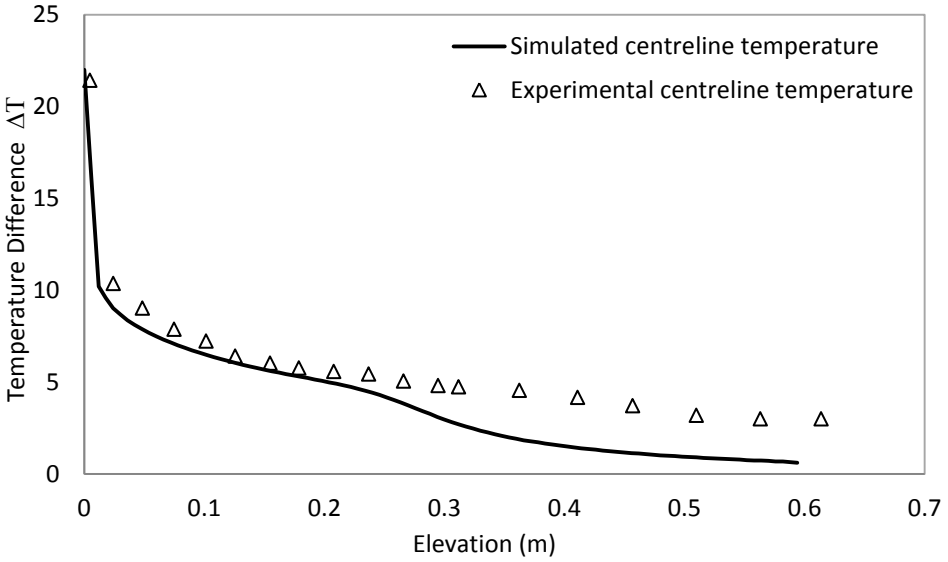

Figure 4.4 Comparison of experimental and simulated centerline temperature profile

Another source of Validation of the model was the comparison of Normalized circulation at *0.2R* elevation with heated plate temperature of $100°C$ and at a vane angle of 30° for normalized radial positions as obtained experimentally by Simpson's et.al. [12]. Circulation was calculated using the equation (3-6).

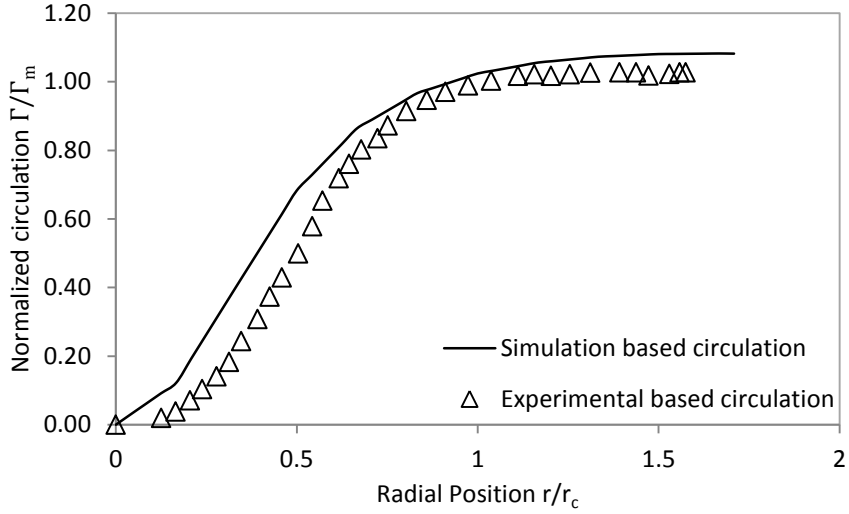

Figure 4.5 Comparison of experimental and simulated circulation at 0.2R elevation

The characteristic radius of the vortex (r_c) is selected at the region where the circulation becomes radially-invariant. The circulation distribution is normalized by the maximum circulation Γ_m, and the tangential velocity was normalized by the peak velocity $V_{\theta m}$, Figure 4.6 and Figure 4.5 show the corresponding normalized radial distributions of the time-averaged tangential velocity $V(r)$ and circulation (Γ_r) of the experimental and steady state values of the simulated results for comparison. The circulation is nearly constant in the outer region and it stays constant up-to the core radius and then starts decaying towards the center for both simulated model and experimental setup.

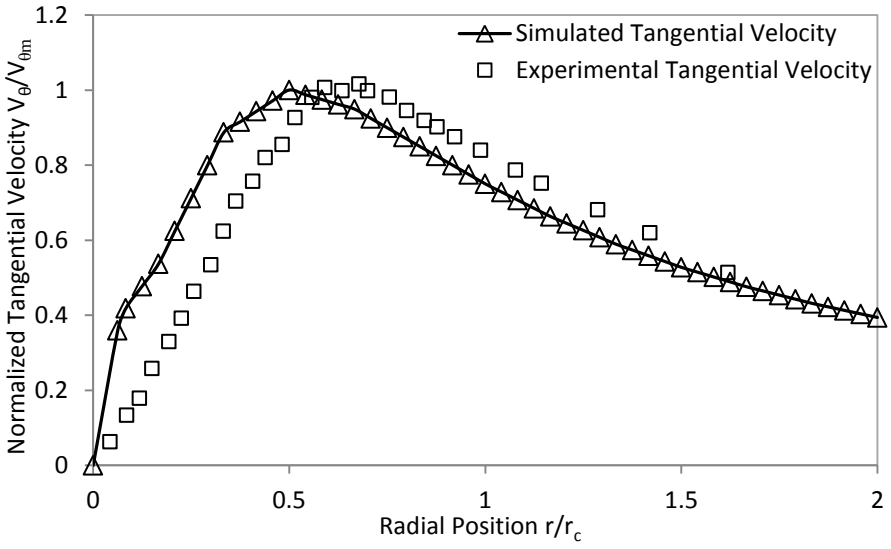

Figure 4.6 Comparison of experimental and simulated tangential velocity at 0.2R elevation

Tangential velocities show a similar trend as that was observed in Figure 4.3 . The simulated results of centerline temperature profile, normalized circulation and tangential velocity show good agreement with the experimental results which implies that numerical model is capable of simulating the flow field.

CHAPTER 5

5. PARAMETRIC STUDY OF GEOMETRIC FACTORS

Following study is carried out to find the effects of vane height, vane width, and vane spacing and vane angle and temperature differences for a particular radius. Before any up-scaling of the geometry it is proposed that the geometry must first be optimized with respect to the length scale, (which is radius R in this case taken as 0.5 m), to achieve maximum flow. After the selection of the optimized geometry the effects of geometrical scaling and temperature differences were observed and a power law relation was developed.

5.1. Effects of vane width

Four simulations were performed with same grid sizing and physical conditions such as plate temperature, ambient temperature, radius of heated plate, number of vanes , vane height and vane angle. Optimization of vane width was started from a vane width of 0.4 R and was increased until no further improvement was observed in the axial volumetric flow rate. The variation of axial volumetric flow rate, when width is changed can be seen in the Figure 5.1 .

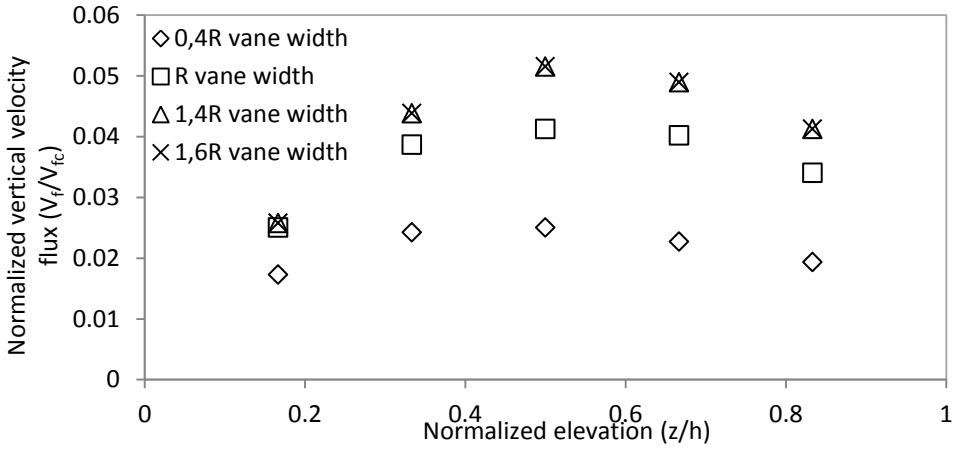

Figure 5.1 Variations of axial velocity with respect to the scaled vane widths.

The axial volumetric flow rate profile improves when vane width is increased. It is noted that after 1.4 R improving the vane width did not change the axial volumetric flow rate profile. The peak axial volumetric flow rate was observed at 0.6R or a normalized elevation of 0.5 for all cases.

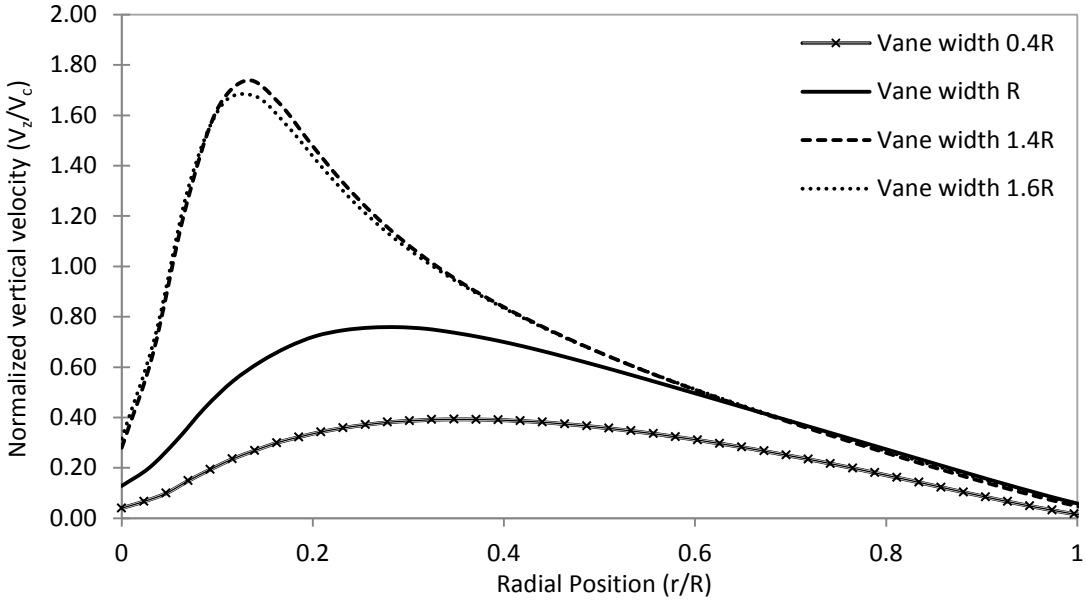

Figure 5.2 Variation of normalized axial velocity with respect to the scaled vane widths at elevation of 0.6R or 0.5 (z/h) for different vane widths

Thus axial velocity at an elevation of 0.6 R was selected as a reference in Figure 5.2. It can be seen in the Figure 5.2 which shows that an elevation of 0.6R, increase in the vane width improved the magnitude of the axial velocity but after a vane width of 1.4R, any further increase in vane width resulted in a very little improvement. This means that 1.4R should be taken as the optimized vane width for that particular radius.

5.2. Effects of vane height

Six simulations were performed with same grid sizing and physical conditions such as plate temperature, ambient temperature, radius of heated plate, number of vanes , vane width and vane angle. Variation of vane height was started from a vane height of 0.6 R and was increased until no further improvement was observed in the axial velocity. For a complete picture axial

volumetric flow rate can be seen in Figure 5.3. It is evident that increasing the vane height improves the axial volumetric flow rate, although the increment between 1.2 R to 1.4 R is more significant and after that it again improves but not significantly from 1.4 R.

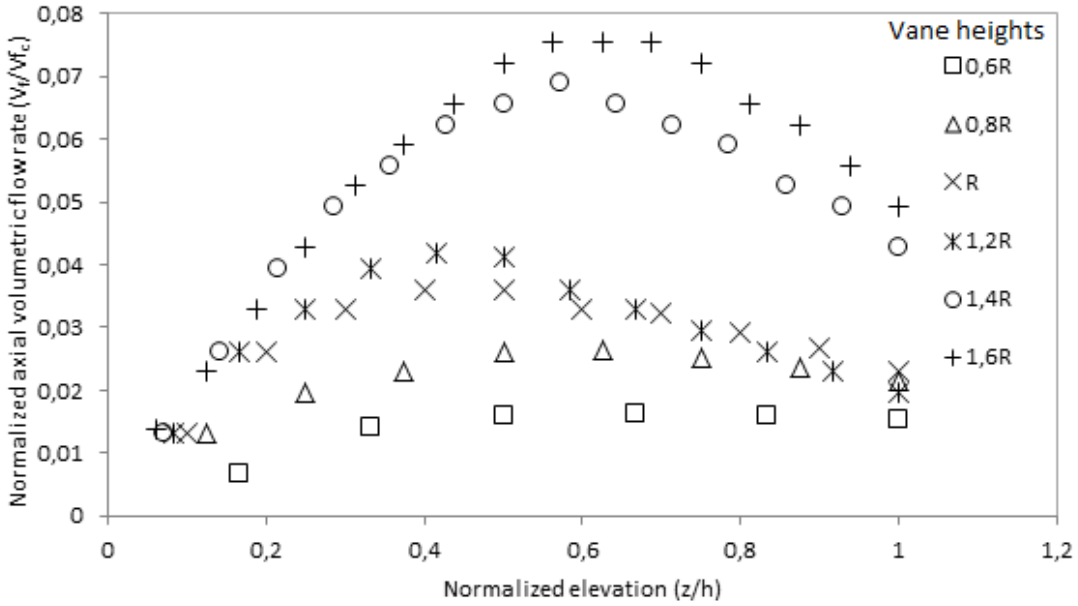

Figure 5.3 Variations of axial volumetric flow rate for different scaled vane heights

Axial velocity at an elevation of 0.2R was selected as a reference. It can be seen in the Figure 5.4 that an increase in the vane height improved the magnitude of the axial velocity but after a vane height of 1.4R, any further increase in vane height resulted in a very little improvement and the axial velocity profile of 1.4R and 1.6R are overlapped in the radial inflow region. This means that 1.4R can be taken as the optimized vane height for that particular radius if the region after the peak can be enclosed or covered to stabilize the flow.

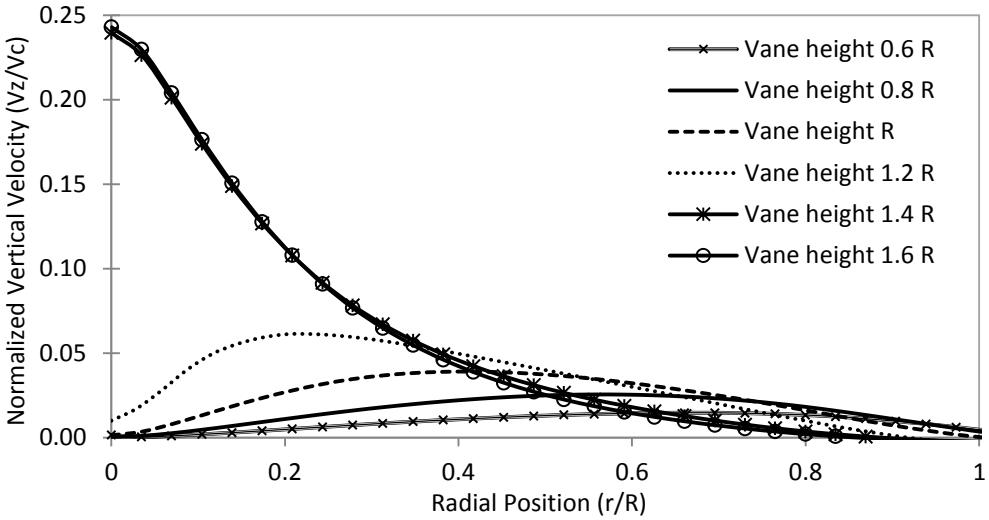

Figure 5.4 Variations of axial velocity with respect to the scaled vane heights

In order to compare all these cases the elevations were selected at respective peak axial volumetric flow rates as shown in Figure 5.5 and in the inflow region vertical velocities were plotted at an elevation of 0.2R in Figure 5.4.

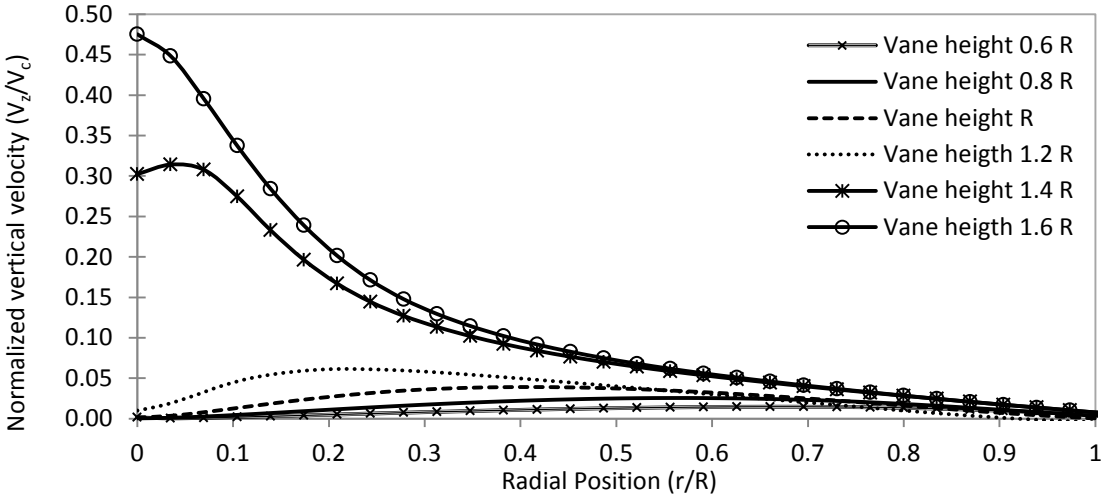

Figure 5.5 Variations of axial velocity at elevations of peak axial volumetric flow rate with respect to the scaled vane heights

By looking at above figures it can be inferred that increasing the vane height increases the peak axial volumetric flow rate. Increasing more than 1.4R does not result in improvement in the region near the plate but it still improves the axial velocity profile in the peak region.

5.3. Effects of vane spacing/number of vanes

The effect of total number of vanes on the axial volumetric flow rate was observed by performing three simulations with, 06, 12 and 18 vanes. Other conditions including grid sizing and physical conditions such as plate temperature, ambient temperature, radius of heated plate, vane height, vane width and vane angle were kept same for all three simulations. Again for this case axial volumetric flow rate variations were plotted for three cases in Figure 5.6. It can be seen that axial volumetric flow rate profile is better for 12 vanes as it is higher than the rest and shows more stability.

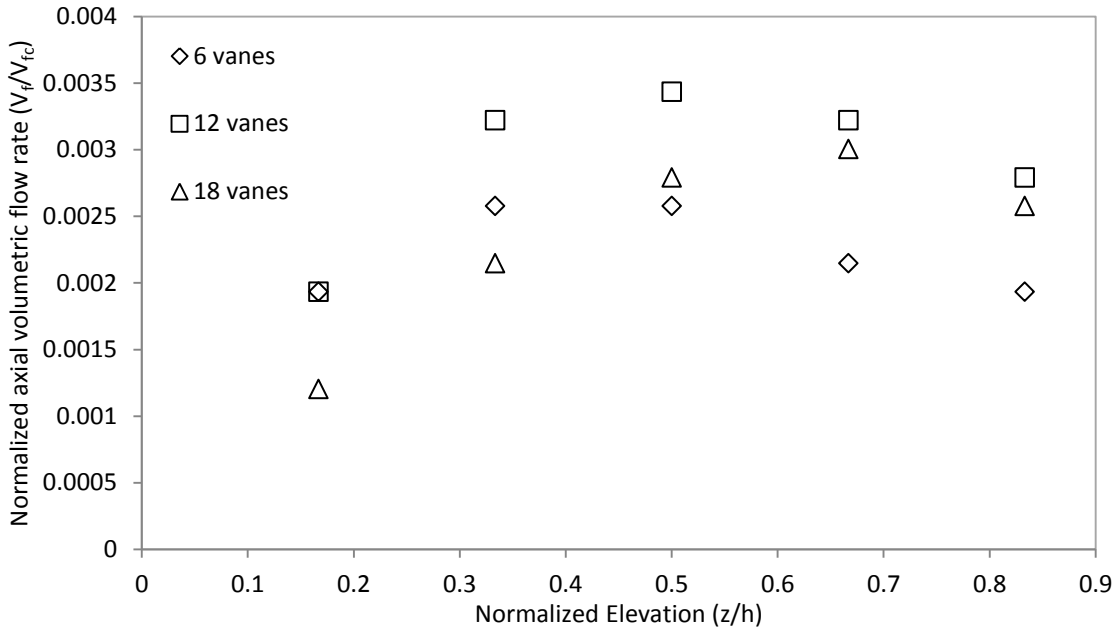

Figure 5.6 Vertical variations of normalized axial volumetric flow rate for different number of vanes

The peak axial volumetric flow rate was found different for three cases, it is noted that increasing the number of vanes shifts the location of peak flow rate upward. In order to compare the axial velocities for three cases the elevations of the peak axial volumetric flow rate were selected. Although increasing the number of vanes favors the formation of the plume as it can be observed by Figure 5.7 but increasing more than 12 vanes does not result in any

significant improvement in the magnitude of axial velocity at the center as it can be seen that velocity profile with 18 vanes is very close to velocity profile with 12 vanes.

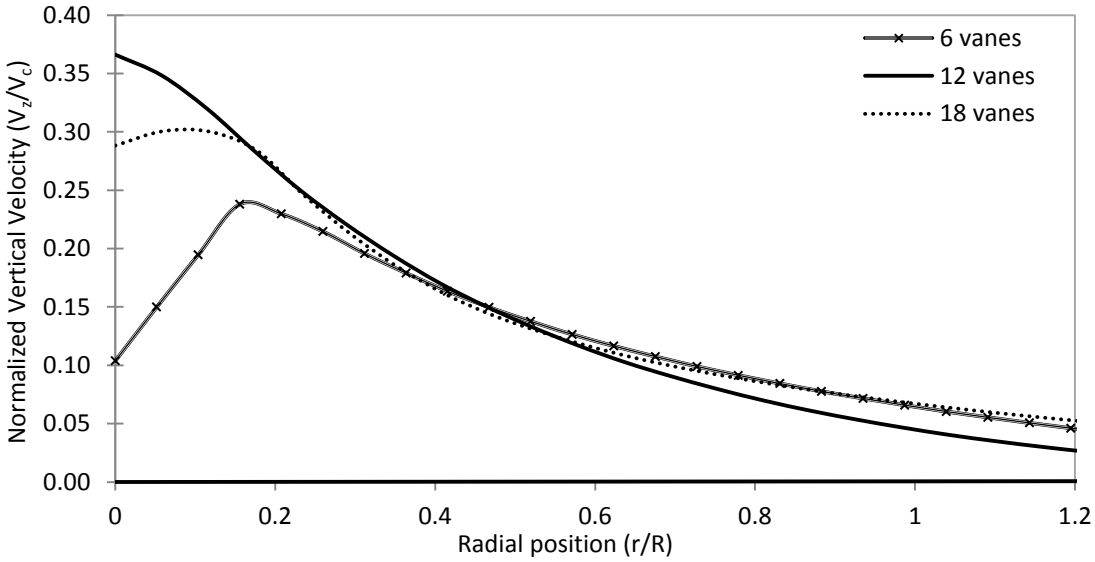

Figure 5.7 Variations of normalized axial velocity in radial direction with respect to the number of vanes at an elevation of respective peak axial volumetric flow rate

5.4. Effects of vane angles

Keeping the temperature difference between the heated plate and the ambient temperature and radius of the plate, vane width and vane height same, the effects of change of vane angles on the vertical and tangential velocities were observed by running the simulations with different vane angles. The axial volumetric flow rate variation is shown in Figure 5.8 . It is interesting to note that at same vane heights and widths and spacing only by changing the vane angles the axial volumetric flow rates can be increased. At lower elevations the axial volumetric flow rates are same for all angles but at higher elevations differences are notable.

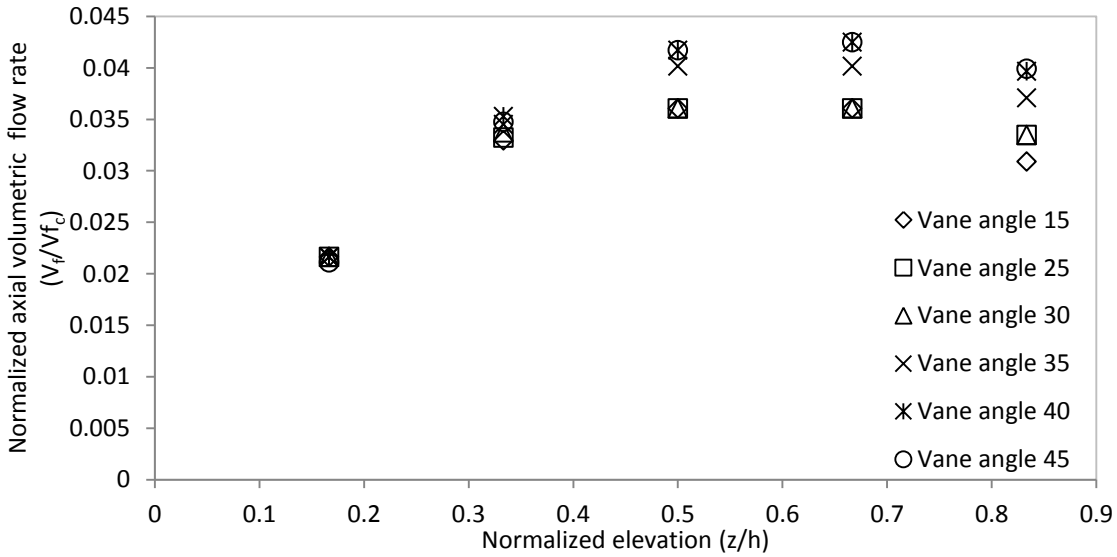

Figure 5.8 Variation of normalized axial volumetric flow rate with elevation for vane angles 15°-45°

It is also to be noted that the axial volumetric flow rate increases at first with elevation and then it starts decreasing again. Before this transition happens, there is a region where the slope of the curve of axial volumetric flow rate is almost zero, which suggests the stability of the vortex. Figure 5.9, Figure 5.10, Figure 5.11 show the tangential, vertical velocity and temperature profiles at an elevation of around 0,2R which is the point where axial volumetric flow rates are almost same.

As it can be seen in the Figure 5.9 at lower vane angles the velocity profile is similar as the formation of a central plume i.e. vertical velocity increases towards the center and its maximum at the center. When vane angles are increased this pattern is gradually changed and the velocity starts decreasing near the center. It can be observed that axial velocity is still approximately same for all cases near the entrance region, and it stays same, up to half the radius of the heated plate. It can be suggested that for maximum yield of energy the flow regime with peak values away from center would be more suitable, because of the increased length of the moment arm of the force applied by the air flow.

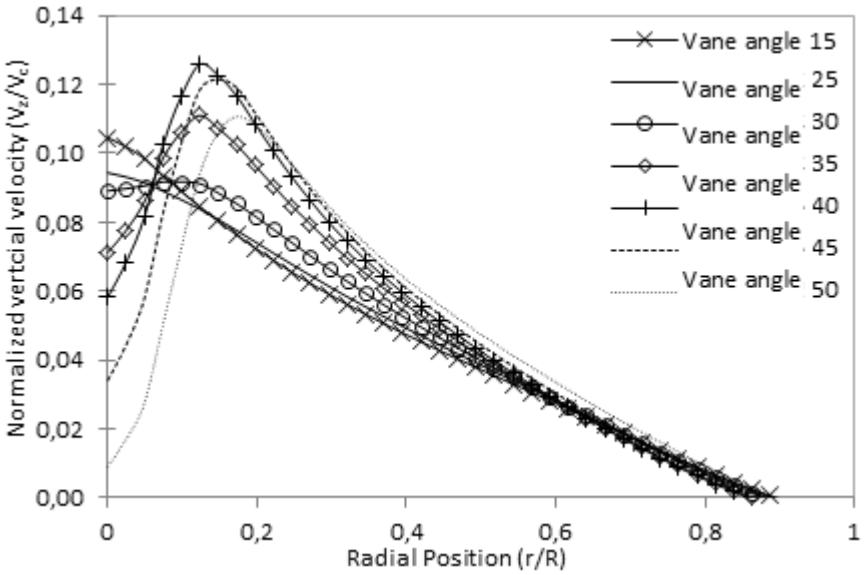

Figure 5.9 Normalized vertical velocity at various vane angles at the elevation of 0.2 R

Similar data was obtained for the tangential velocity at the same elevation and it can be seen in the Figure 5.10 which shows the variation of tangential velocity in the radial direction for various vane angles. It can be seen that tangential velocity is higher at higher vane angles. Generally the tangential velocity starts increasing from the entrance and it reaches a peak value and then it starts decreasing again. The peak tangential velocity is also higher for higher vane angles.

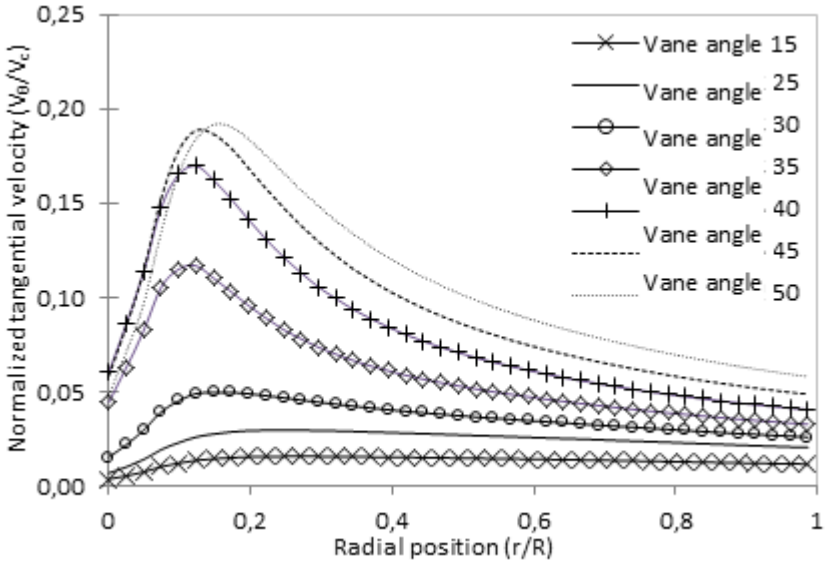

Figure 5.10 Tangential velocity for various vane angles at the elevation of 0.2 R

Variation of Vertical velocities and tangential velocities with respect of vane angles at this elevation 0.2 R can be explained considering conservation of energy principle. As the source of energy i.e. heated plate is same and the amount of input energy available is same for all cases, so assuming that total energy in all cases is same, it can be said that as the vane angles are increased the kinetic energy present in tangential component of velocity near entrance region is higher than the kinetic energy present in the vertical component of velocity near the center. This goes vice versa. As the vane angles are decreased the kinetic energy present in vertical component of velocity near center region is higher than the kinetic energy present in the tangential component of velocity near the entrance region. It can be seen that having higher vane angles resulted in higher tangential velocities at the elevation of 0.2R which shows the strengthening of the vortex and which in turn improved the axial volumetric flow rate at higher elevations.

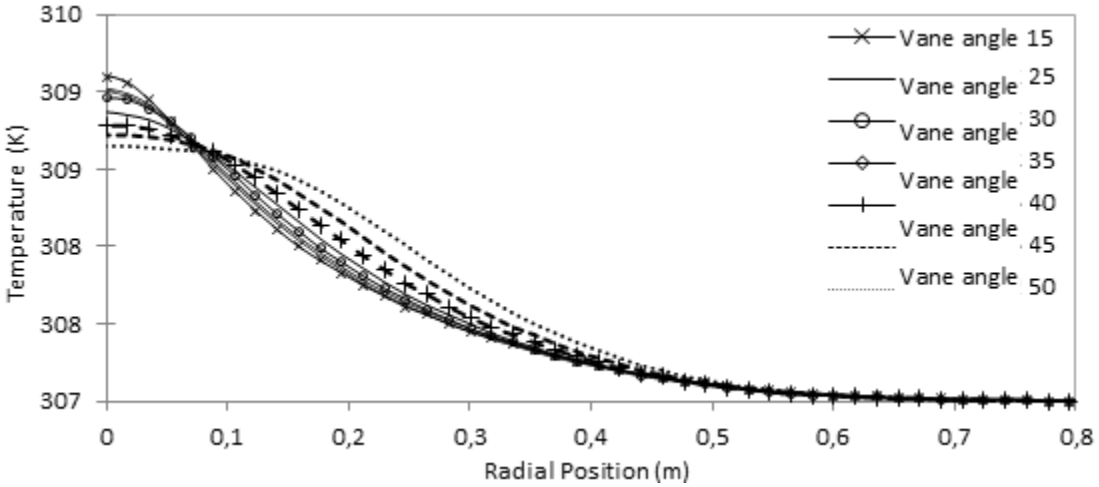

Figure 5.11 Temperature profile at the elevation of 0.2 R for different vane angles

There is an observable pattern in the temperature profile as shown in Figure 5.11. Low vane angles result in a sharp peak of temperature and as the vane angles are increased the sharp peak converts into a domed peak. The maximum temperature also decreases with the increase in vane angle. At entrance region the temperature is higher for lower vane angles and is lower for higher vane angles. At center region happens exactly opposite of entrance region. This temperature profile suggests that energy content is concentrated in the center region for lower vane angles and the energy content is more evenly distributed in case of higher vane angles which favors the energy extraction.

Based on Figure 5.8 the elevations for peak axial volumetric flow rate were selected and by using equation (3-8) peak averaged axial velocities were calculated and plotted in following Figure 5.12 for various vane angles. The peak average velocity did not increase much between two lower and upper vane angles but in between there is an increasing trend. This analysis suggests that there could be an optimum range of vane angles for a particular geometry and beyond which the peak average axial velocity does not increase.

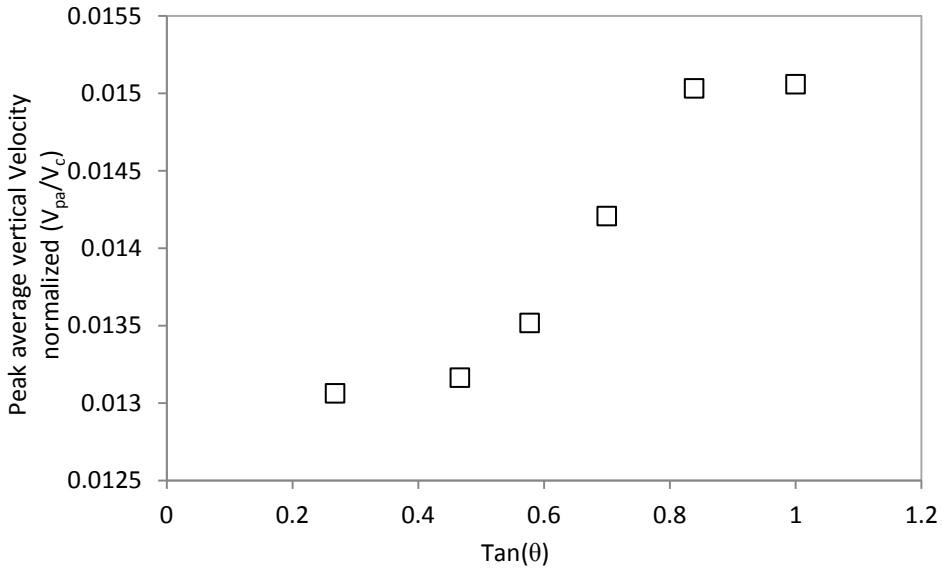

Figure 5.12 Normalized peak average axial velocity vs. tangent of various vane angles

The elevations of peak axial volumetric flow rate were selected for all vane angles to plot the axial and tangential velocities in Figure 5.13 and Figure 5.14. At these elevations the magnitudes of axial velocities are comparably higher than tangential velocities which can also be observed in Figure 5.15 in the form of swirl number which is lower at these elevations.

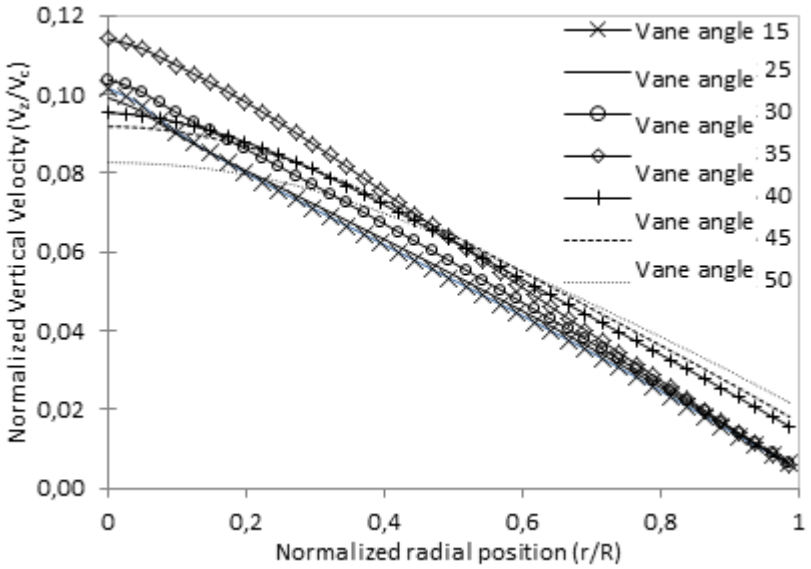

Figure 5.13 Normalized peak axial velocity vs. radial position for different vane angles

The peak axial velocities depicted in Figure 5.13 show that for 45° and 50° vane angles the vertical velocity values are higher away from center and for 35° vane angle the values are higher near the center region. It can be said that looking into peak axial volumetric flow rate are not enough for a complete analysis, the velocity profiles are also necessary to be considered. For instance, in this case having higher values away from center are favorable which in this case are at 45° and 50° vane angles.

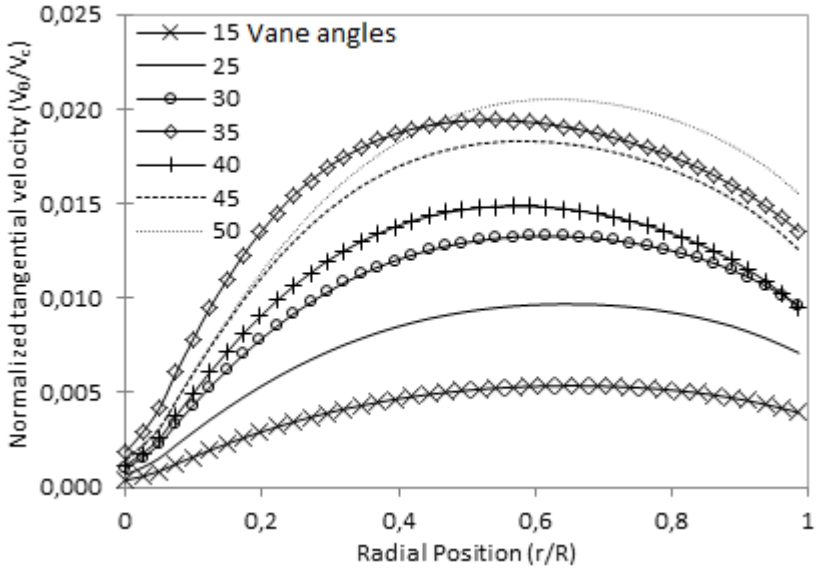

Figure 5.14 **T**angential velocity vs. radial position for different vane angles at elevation of peak axial volumetric flow rate

Although the magnitudes of the tangential velocities are low as seen in the Figure 5.14 and also as shown by their low swirl numbers, but the tangential velocity magnitudes for higher vane angles are again higher away from center.

Swirl number S_w was measured and plotted against scaled elevation levels for different vane angles in Figure 5.15 . Swirl number is higher at lower elevations for each vane angle and it reduces in upward direction. Swirl number provides a comparison between the tangential and axial components of velocities at a particular elevation. This information could be useful in determining the angle of attack of the turbine blade. The angle of attack can be adjusted to be exposed to tangential component more when swirl number is high. When the swirl number is

low, the angle of attack can be adjusted to increase the exposure of axial component of the velocity to the turbine blade to extract more power.

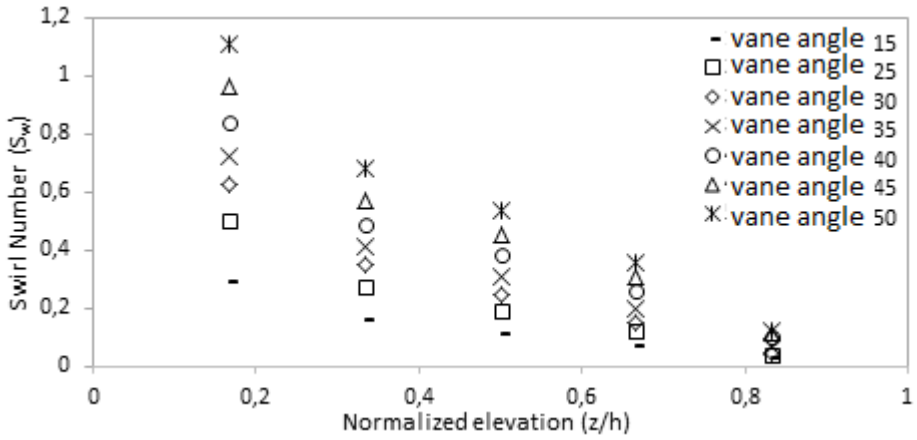

Figure 5.15 Variation of swirl number with elevation for various vane angles

5.5. Combined effects of vane height, width and spacing

In order to observe the effects of selected optimized parameters of vane width, vane height and number of vanes, two simulation were conducted with selection of 1.4R width, 1,6R height and 12 vanes and R width, 1,6R height and 18 vanes. These simulations were compared with the previous simulations 1.4R width 1.2R height 12 vanes and 0.8R width 1.2R height and 12 vanes. Figure 5.16 shows the axial volumetric flow rates for four cases. Out of four different combinations the forth one, is best because firstly the peak flow rate is higher than all other cases, secondly the slope after the inflow region is also close to zero which shows the stability of the flow.

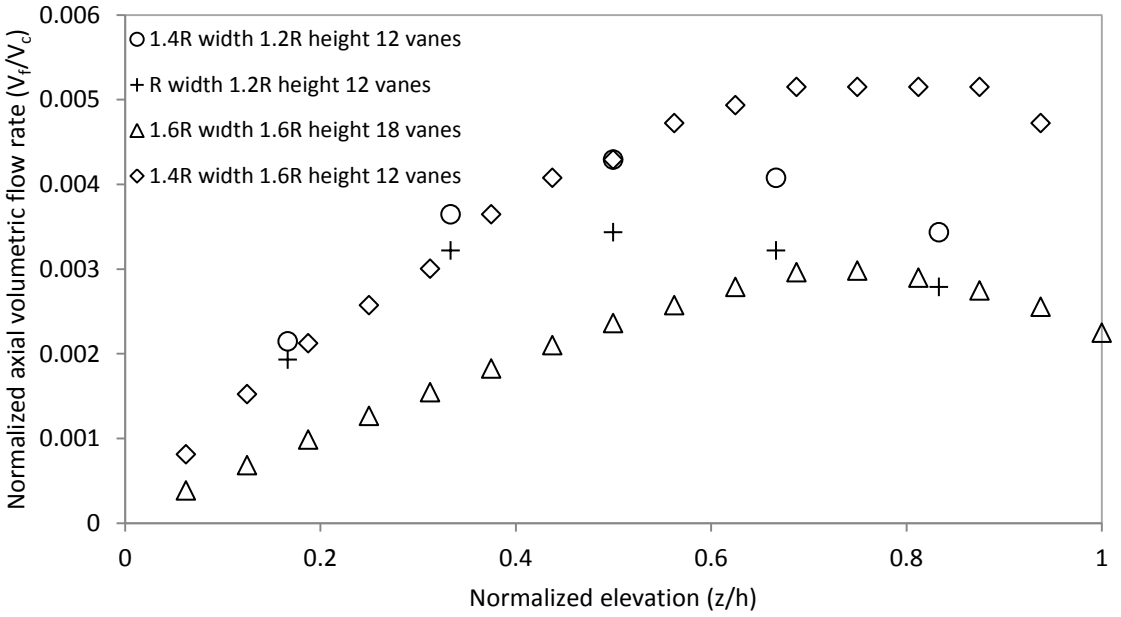

Figure 5.16 Tangential velocity for various vane angles at the elevation of 0.2 R

Figure 5.17 shows the axial profile of all cases with respect to the optimized geometry at elevations of peak axial volumetric flow rate. Combining optimized geometrical features certainly does result in the strengthening of the central plume, as shown by the increased centerline axial velocity; also the potential of energy extraction of this setting depends on the magnitude and the profile of the velocity at that elevation which is also improved for the optimized geometry.

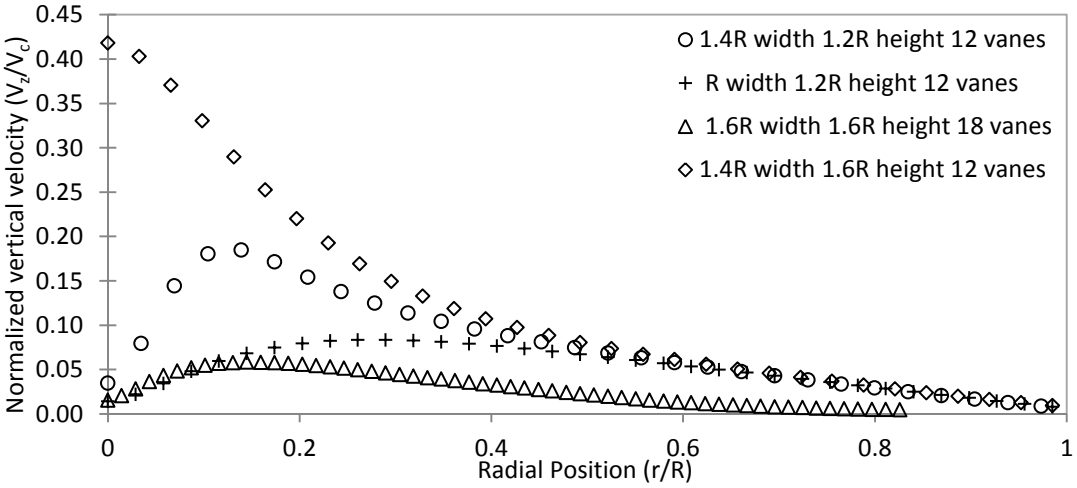

Figure 5.17 Combined effects of optimization of all parameters

5.6. Effects of temperature difference

Based on the last discussion the selected geometry with parameters as shown in Table 5.1 with radius equal to 0.5 m was simulated for various heated-plate/ambient temperature differences ranging from 12° to 20°. As it was expected it can be seen in Figure 5.18 that in the region of the radial inflow, the axial volumetric flow rates look similar for all cases but there are differences in the decay region which are that with the increase of temperature differences, axial volumetric flow rates show an increasing trend in the decay region. The vertical location of the peak axial volumetric flow rate also stays the same for all cases.

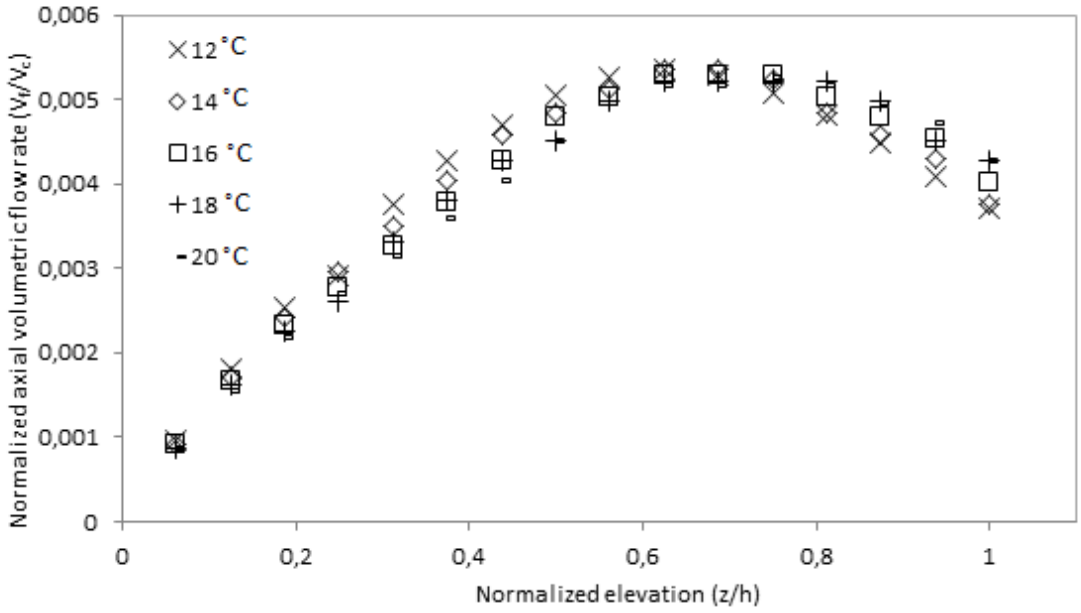

Figure 5.18 Variation of axial volumetric flow rate with elevation for different temperature differences

The elevations of peak volumetric flow rates were selected which in this case were equal to the radius R of the heated plate and for a comparison axial velocity profiles were plotted in Figure 5.19 to understand the differences in the axial velocities. It is observed that velocity magnitudes increase in the central region and the magnitudes are quite similar in the regions away from the center. Thus it can be concluded that by increasing temperature differences, energy concentration in the center region increases.

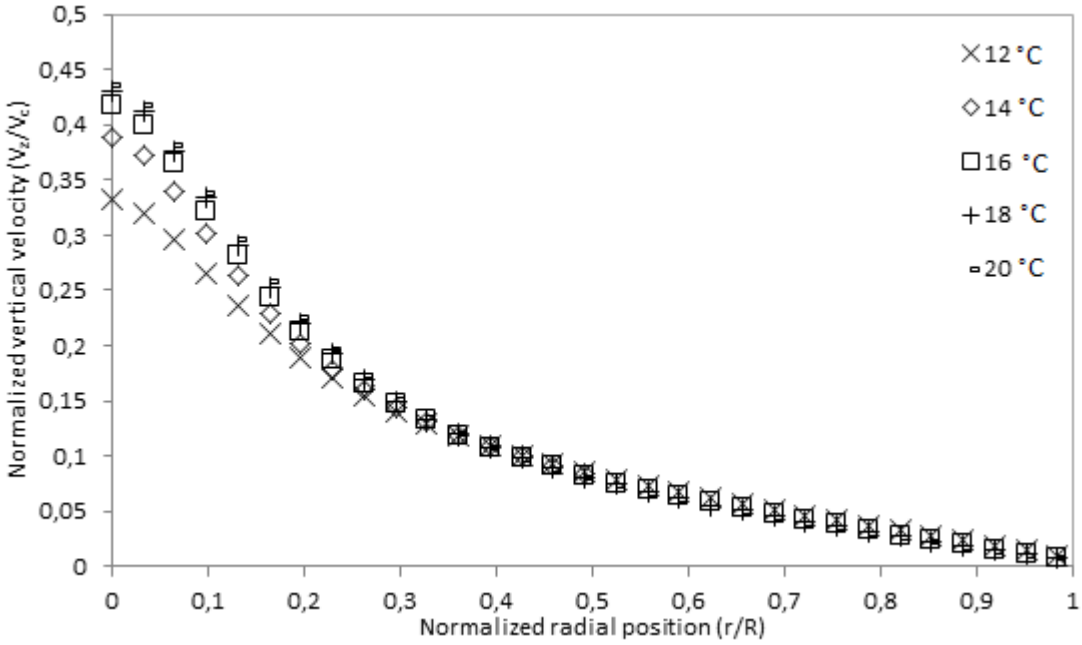

Figure 5.19 Normalized vertical velocities vs. radial position for same geometries at elevation R for different temperature differences

Peak axial volumetric flow rates were selected for all cases and average vertical velocities V_{pa} were obtained by dividing the volumetric flow rates with respective cross sectional area of the flow. These peak vertical velocity values were plotted in Figure 5.20 along the temperature differences and a power law curve was fitted.

Following relation as shown in equation (5-1) was obtained for the peak average vertical velocity and temperature difference ΔT.

$$\frac{V_{pa}}{V_c} = 0.4518 \left(\frac{\Delta T}{T_\infty}\right)^{0.5} \tag{5-1}$$

This relation suggests that velocity and temperature difference ratio have a relation of a square-root.

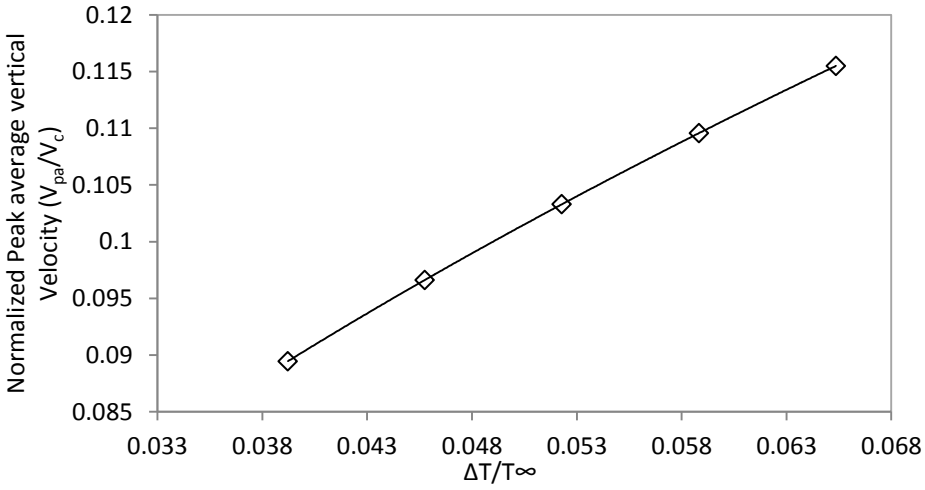

Figure 5.20 Peak average vertical velocity vs. temperature differences for same geometry

5.7. Effects of up-scaling and downscaling

Keeping the temperature constant, and maintaining the geometrical similarity as it is shown in Table 5.1 ,the whole system was up-scaled and downscaled within a range of S = 0.6 to 1.4. The base case for the scaling factor is the case with 0.5 m heated plate radius hence R_{ref} is 0.5 m in this case. The scaling factor S thus can be defined as follows.

$$S = R_s/R_{ref} \tag{5-2}$$

Table 5.1 Geometrical Parameters for geometric similarity

Geometrical parameter	**Value**
Radius of heated plate ($\boldsymbol{R_s}$)	r
Height of the vanes (h)	$1.6r$
Width of the vanes ($\boldsymbol{c}$)	$1.4r$
Angular span ($\boldsymbol{\Phi}$)	30˚
Number of vanes	12

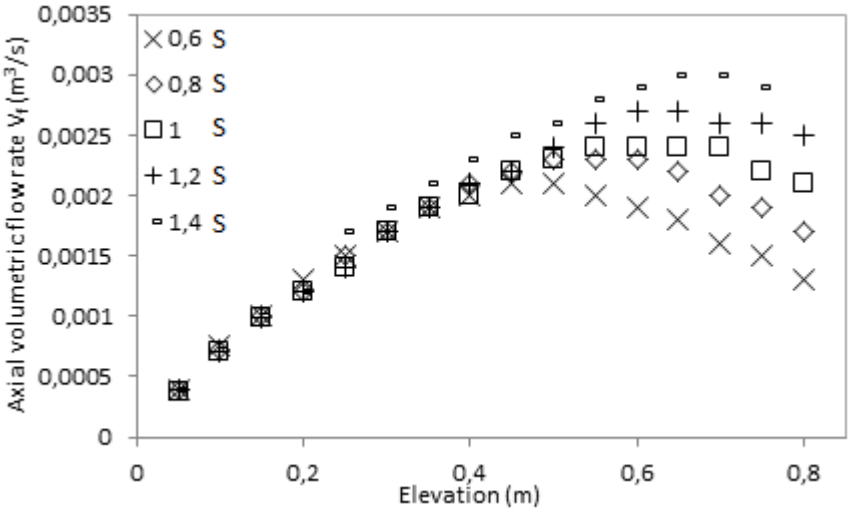

Figure 5.21 Variation of axial volumetric flow rate with elevation for different geometric scales 0.6-1.4 (S)

Figure 5.21 shows effects of scaling on the axial volumetric flow rate. Generally the variation of axial volumetric flow rate is negligible in the inflow region and the differences are prominent in the decay region.

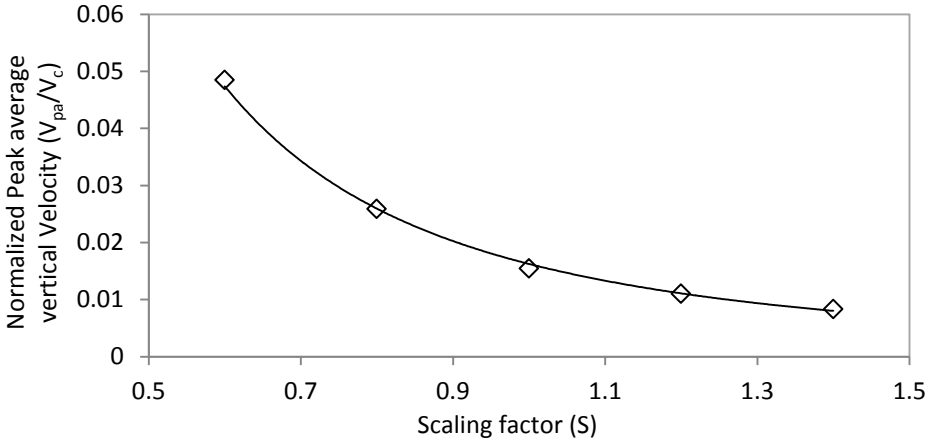

Figure 5.22 Variation of peak average vertical velocity with elevation for scaling

The trend in decay region shows an increase of axial volumetric flow rate with scale factor S. The peak volumetric flow rate for each case were used to find the average peak velocity by

dividing the volumetric flow rate with the respective cross sectional flow area as discussed in equation (3-8). These peak velocities were plotted with respect to the scale S in Figure 5.22 .A power law curve was fitted on the plot and following relation as shown in equation (5-3) was obtained which shows a relation of power of – 2 between the geometric scale of the system and the peak average vertical velocity.

$$\frac{V_{pa}}{V_c} = 0.0163\, S^{-2} \tag{5-3}$$

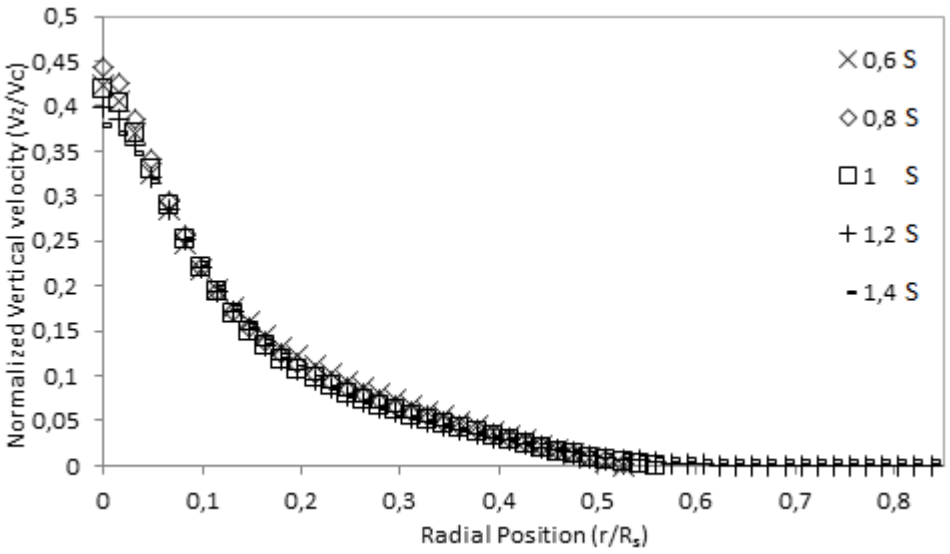

Figure 5.23 Variation of vertical velocity with radial position for different scales

Another measure is to compare the actual axial velocities at the elevations of peak axial volumetric flow rates . Figure 5.23 contains the plot of vertical velocities in the radial direction. Although the average peak velocities decrease with the up-scaling of the geometry, it can be noted that the magnitudes of the peak axial velocities near the center increase with up-scaling which means that with increasing dimensions of the system the concentration of energy in the center is also increasing. Although this increase is overall favorable for the extraction of power via wind turbine but the velocity magnitudes away from center would produce more power due to increase in the moment arm of the applied drag, though in these cases the magnitudes away from the center decrease with geometric up-scaling. This suggests that upscaling would require increase in the vane angles so that this kinetic energy near the center could be shifted from the

center in the form of axial velocities to tangential velocities away from the center which will yield more power because of the increase of the moment arm. This means that upscaling should be supplemented by increasing the vane angles. Further studies should be performed by using geometrical scaling with higher vane angles and the obtained velocity profiles should be used to estimate the obtainable power to find the co-relation between power and geometric scale.

5.8. Summary of the chapter

A parametric study was conducted to help in the optimization of the geometry. This parametric study was carried out to study the effects of variation of physical parameters such as number of vanes, vane angles, vane height, vane width, on axial volumetric flow rates of similar length scale (radius R). Axial volumetric flow rate with respect to elevation were plotted for several cases. It was found that axial volumetric flow rate can be increased by increasing the vane heights and increasing the vane width up to the length scale of 1.4 R. It was also found that there was an optimum vane spacing which is acquired by placing 12 vanes. An optimized geometry was selected from the results of above cases and the effects of increase in temperature differences and geometrical up-scaling were observed. The axial volumetric flow rates were plotted and peak volumetric flow rate elevations were selected. These peak volumetric flow rate elevations were used to infer the relation between the temperature difference and peak average velocities, and scaling factor S and peak average velocity. It was observed that for same geometry temperature difference affects the flow with a power of square-root and scaling factor S effects with a power of -2. Furthermore it was observed that increasing the vane angle increased the magnitude of tangential velocities and caused a decrease of vertical velocity at the central region. There is an optimum range of vane angles beyond which or before which the variations in axial volumetric flow rate are negligible.

CHAPTER 6

6. CONCLUSION

6.1. Thesis conclusions

A numerical model was developed using OpenFOAM, based on an existing experimental setup. The geometry used in this study is simply a circular heated plate surrounded by azimuthally placed vertical vanes. A simplified grid was developed by applying cyclic boundary condition to reduce the computational time, memory space and post processing time. After the selection of the grid style, grid refinement strategy was developed to avoid unnecessary grid refinement in regions which are not focused in this study. The transient solver used in this study assumes incompressible flow and density variations were accounted using boussinesq`s approximation. Thermo-physical properties were modeled using a pressure temperature system from which other properties are calculated using an ideal gas model defined by fluids molecular mass, M, and constant specific heat, c_p [40]. Transport properties such as dynamic viscosity, μ and thermal diffusivity,α are computed using constant values for fluid's kinematic viscosity,$\nu = \mu/\rho$ and Prandtl number $= \nu/\alpha$. Turbulence modeling was based on standard $k - \varepsilon$ model. A grid convergence study was performed to check the order of accuracy in terms of discretization errors. After the development of the numerical model, validation studies were carried out based on the results of previous experimental and theoretical models. It was found that a vortex forms at the center region and the simulated results are in good agreement with the experimental results.

After the validation studies a parametric study was conducted to extend the understanding of the effects of the geometrical and physical factors. This parametric study was carried out to study the effects of variation of geometrical parameters such as number of vanes, vane angles, vane height, vane width, on axial volumetric flow rate profiles of similar heated plate length scale (radius R). It was found that axial volumetric flow rate can be increased by increasing the, vane heights and increasing the vane widths up to the length scale of 1.4 R. An optimized geometry was selected from the results of above cases and the effects of increase in

temperature differences and geometrical up-scaling were observed. The axial volumetric flow rates were plotted and peak volumetric flow rate elevations were selected. These peak volumetric flow rate elevations were used to infer the relation between the peak average velocities, and temperature differences / scaling factor S. It was observed that for same geometry, temperature difference affects the peak average axial velocity of the flow with a power of square-root and scaling factor S affects peak average axial velocity of the flow with a power of -2. Furthermore it was also observed that increasing the vane angle increased the magnitude of tangential velocities and caused a decline of vertical velocity at the central region. Finally it can be concluded from the parametric study that an optimum width and vane spacing can be suggested for a particular scale of the setup while vane angles in the optimum range can be used to redistribute the concentration of energy from the center to the distances away from center for higher yield of energy. Geometric up-scaling although increases the concentration of energy in the center region, but away from the center it`s exactly opposite, that is why geometric up-scaling should be supplemented with higher vane angles. Similar is the case with temperature differences, increasing the temperature difference increases the concentration of energy in the center and higher vane angles should supplement the higher temperature differences.

6.2. Future work

In general numerical modeling can provide an opportunity to simulate the physical world experiments at ease and it provides flexibility to choose the physical conditions as per the requirement. Motivations for further research into this numerical model of the experimental setup may be other than for power generation opportunities such as modeling of terrestrial and Martian dust devils, opportunities of heat transfer enhancement via addition of vanes on a heated plate for cooling purposes or to extend the research in the area of vortex dynamics. Further improvements in numerical model are possible by utilizing and comparing the results with commercial soft-wares or by development of experimental setups to acquire more data for validation.

REFERENCES

[1] P. C. Sinclair, “The Lower Structure of Dust Devils,” J. Atmos. Sci., vol. 30, no. 8, pp. 1599–1619, Nov. 1973.

[2] P. C. Sinclair, “General Characteristics of Dust Devils,” *J. Appl. Meteor.*, vol. 8, no. 1, pp. 32–45, Feb. 1969.

[3] M. R. Balme, A. Pathare, S. M. Metzger, M. C. Towner, S. R. Lewis, A. Spiga, L. K. Fenton, N. O. Renno, H. M. Elliott, F. A. Saca, T. I. Michaels, P. Russell, and J. Verdasca, “Field measurements of horizontal forward motion velocities of terrestrial dust devils: Towards a proxy for ambient winds on Mars and Earth,” *Icarus*, vol. 221, no. 2, pp. 632–645, Nov. 2012.

[4] M. Balme and R. Greeley, “Dust devils on Earth and Mars,” *Rev. Geophys.*, vol. 44, no. 3, p. RG3003, 2006.

[5] D. M. Tratt, M. H. Hecht, D. C. Catling, E. C. Samulon, and P. H. Smith, “In situ measurement of dust devil dynamics: Toward a strategy for Mars,” *J. Geophys. Res.*, vol. 108, no. E11, p. 5116, 2003.

[6] J. C. Kaimal and J. A. Businger, “Case Studies of a Convective Plume and a Dust Devil,” *J. Appl. Meteor.*, vol. 9, no. 4, pp. 612–620, Aug. 1970.

[7] N. O. Rennó, M. L. Burkett, and M. P. Larkin, “A Simple Thermodynamical Theory for Dust Devils,” *J. Atmos. Sci.*, vol. 55, no. 21, pp. 3244–3252, Nov. 1998.

[8] N. O. Rennó and H. B. Bluestein, “A Simple Theory for Waterspouts,” *J. Atmos. Sci.*, vol. 58, no. 8, pp. 927–932, Apr. 2001.

[9] N. O. Renno, V. J. Abreu, J. Koch, P. H. Smith, O. K. Hartogensis, H. A. R. De Bruin, D. Burose, G. T. Delory, W. M. Farrell, C. J. Watts, J. Garatuza, M. Parker, and A. Carswell, “MATADOR 2002: A pilot field experiment on convective plumes and dust devils,” *J. Geophys. Res.*, vol. 109, no. E7, p. E07001, 2004.

[10] R. Lorenz and M. Myers, “Dust devil hazard to aviation: A review of United States air accident reports,” *J. Meteor*, vol. 30, pp. 178–184, 2005.

[11] D. E. Fitzjarrald, “A Laboratory Simulation of Convective Vortices,” *J. Atmos. Sci.*, vol. 30, no. 5, pp. 894–902, Jul. 1973.

[12] M. W. Simpson, A. J. Pearlstein, and A. Glezer, “Power Generation From Concentrated Solar-Heated Air Using Buoyancy-Induced Vortices,” pp. 585–593, Jul. 2012.

[13] R. K. Smith and L. M. Leslie, "Thermally driven vortices: A numerical study with application to dust-devil dynamics," *Q.J.R. Meteorol. Soc.*, vol. 102, no. 434, pp. 791–804, 1976.

[14] R. Greeley, M. R. Balme, J. D. Iversen, S. Metzger, R. Mickelson, J. Phoreman, and B. White, "Martian dust devils: Laboratory simulations of particle threshold," *J. Geophys. Res.*, vol. 108, no. E5, p. 5041, 2003

[15] G. H. Vatistas, V. Kozel, W. C. Mih 1991, A simpler model for concentrated vortices, Experiments in Fluids Vol 11 no 1 pp 73-76

[16] Kanak, K. M., D. K. Lilly, and J. T. Snow, 2000: The formation of vertical vortices in the convective boundary layer. Quart. J. Roy. Meteor. Soc., 126, 2789–2810.

[17] G. H. Vatistas, V. Kozel, W. C. Mih 1991, A simpler model for concentrated vortices, Experiments in Fluids Vol 11 no 1 pp 73-76

[18] Rankine, W. J. M. 1901 A manual of applied mechanics. 16th Edition. Charles Griffin and Company Limited, London, UK

[19] Burgers, J. M. 1948 A mathematical model illustrating the theory of turbulence. Adv.Appl. Mech., 1, 197–199

[20] Rott, N. 1958 on the viscous core of a line vortex. Z. Angew. Math. Physik, 96, 543–553

[21] GU Zhaolin, QIU Jian, ZHAO Yongzhi, LI Yun, "Simulation of Terrestrial Dust Devil Patterns" *Advances in Atmospheric Sciences,* Vol 25 , NO.1 31-42 ,2008

[22] Lugt, H.J, "Vortex Flow in Nature and Technology", *John Wiley*, New York. 1983

[23] Green, S.I. (1995), Fluid Vortices, Kluwer Acad., Norwell, Mass.

[24] Flower, W. D. 1936 'Sand devils'. Great Britain. Meteorological Office Professional Note 71. Available from Met Office, Exeter, UK

[25] Williams, N. R. 1948 "Development of dust whirls and similar small-scale vortices". Bull. Am. Meteorol. Soc., 29, 106–117

[26] Battan, L. J. 1958 "Energy of a dust devil". J. Meteorol., 15, 235

[27] Bluestein, H. B., Weiss, C. C. and Pazmany, A. L. 2004 "Doppler radar observations of dust devils in Texas". Mon. *Weather Rev*., 132, 209–224

[28] Ward NB. 1972. "The exploration of certain features of tornado dynamics using a laboratory model". *J. Atmos. Sci.* 29:1194–204

[29] Church CR, Snow JT, Agee EM. 1977. "Tornado vortex simulation at Purdue University". *Bull. Am. Meteorol*. Soc. 58:900–8

[30] H. J. Sheen, W. J. Chen,S. Y. Jeng, T. L. Huang "Correlation of Swirl Number for a Radial-Type Swirl Generator", Experimental Thermal and Fluid Science 1996; 12:444-451

[31] Chigier, N. A., and Bedr, J. M., "Velocity and Static-Pressure Distributions in Swirling Air Jets Issuing from Annular and Divergent Nozzles", *J. Basic Eng*. 788-796, December 1964

[32] Yoon, H. K., and Lilley, D. G., Five-Hole Pitot Probe Time-Mean Velocity Measurements in Confined Swirling Flows, AIAA 21st Aerospace Sci. Meeting, Reno, NV, AIAA-83-0315, 1983.

[33] S. B. Robinson, J. A. Liburdy, "Prediction of the Natural Convective Heat Transfer from a Horizontal Heated Disk", *Journal of Heat Transfer*, 906/Vol. 109, NOVEMBER 1987

[34] Kenzo Kitamura , Fumiyoshi Kimura ,"Fluid Flow and Heat Transfer of Natural Convection over Upward-Facing, Horizontal Heated Circular Disks", *Heat Transfer—Asian Research*, 37 (6), 2008

[35] Kenzo Kitamura , Fumiyoshi Kimura ,"Heat transfer and fluid flow of natural convection adjacent to upward-facing horizontal plates" , *Int. Z Heat Mass Transfer*. Vol. 38, No. 17, pp. 3149-3159, 1995

[36] C.J Kobus , G.L Wedekind, "An experimental investigation into natural convection from horizontal isothermal circular disks" , *International Journal of Heat and Mass Transfer*, 44 (2001) 3381-3384

[37] WW. Yousef , J.D Tarasuk, W.J McKeen , "Free Convection Heat Transfer From Upward-Facing Isothermal Horizontal Surfaces" , *Journal of Heat Transfer*, Vol 104/493 August 1982

[38] Massimo Corcione , " Heat transfer correlations for free convection from upward facing horizontal rectangular surfaces" , Wseas Transactions On Heat And Mass Transfer, Manuscript received Jun. 23, 2007; revised Dec. 29, 2007

[39] Kanak, K. M., 2005: Numerical simulation of dust devilscale vortices. Quart. J. Roy. Meteor. Soc., 131, 1271–1292.

[40] P.Sosnowski and J. Pozorski, "Open-source CFD analysis of multi-domain unsteady heating with natural convection" , *TASK Q.Sci.Bull.Acad.Comput.Cent.Gdansk*, Vol 13, pp.403-414, 2009

[41] "OpenFOAM ® Documentation." [Online]. Available : http://www.openfoam.org/docs./ [Accessed :20-Jan-2015]

[42] H.K Versteeg, W.Malalasekkera, "An introduction to computational fluid dynamics The finite volume method", *Longman Scientific and Technical* , 1995

[43] P. J. Roache, "Quantification of uncertainty on computational fluid dynamics" *Annu. Rev. Fluid. Mech*. 1997. 29:123–60

APPENDIX A

INTITIAL MESHING METHOD

An initial grid is generated based on the geometry of the experimental setup of Simpsons et al. A total of 137 blocks are generated with two different categories of blocks.

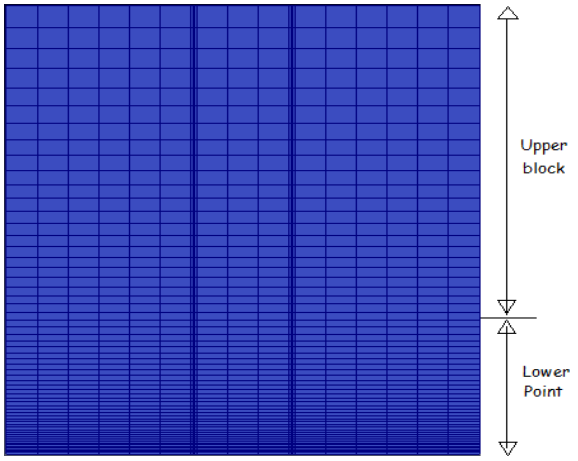

Figure 0.1 Side-view of the upper and lower blocks

The lower set of block consists of 75 blocks. This set of block defines the basic geometry of the setup. It starts from the floor and ends with the vanes. In order to change the vane height only the height of this set of block needs to be changed. This also provides a flexibility to change cell spacing or the total number of cells within the region encompassing the vanes.

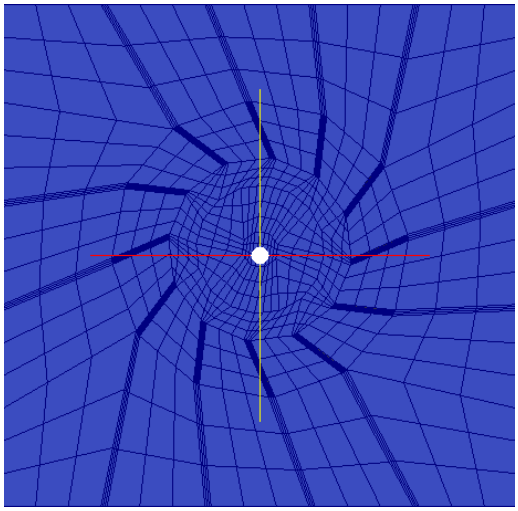

Figure 0.2 Top view of the lower set of blocks

The top view of grid of the set of lower set of blocks can be seen in Figure 0.2 In order to incorporate the vanes the floor is extruded. As it can be seen that for vanes there is just empty space, i.e. no blocks are present. This extruded portion of the floor is defined as a different wall, to apply a different boundary condition on the vanes.

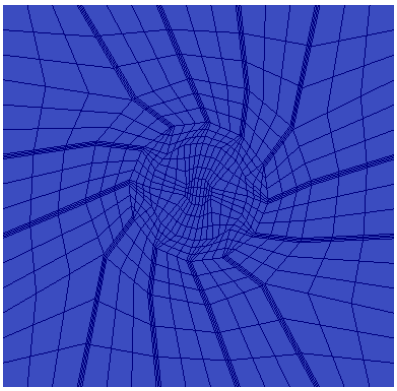

Figure 0.3 Top view of the upper set of blocks

The upper set of blocks contains 87 blocks. The upper set of block is just the replica of lower set of blocks. It is placed just above the lower set of blocks. Here again it provides the same

flexibility of altering the number of cells or the cell spacing as per the requirement. The diameter of the heated plate and the angles, heights and widths of the vanes are adjustable. In this particular simulation the grid contains 12 radially installed vanes of height 60 cm and width 40 cm. The angle was set equal to 30°. The vanes are installed on a heated surface of diameter equal to 1 m.

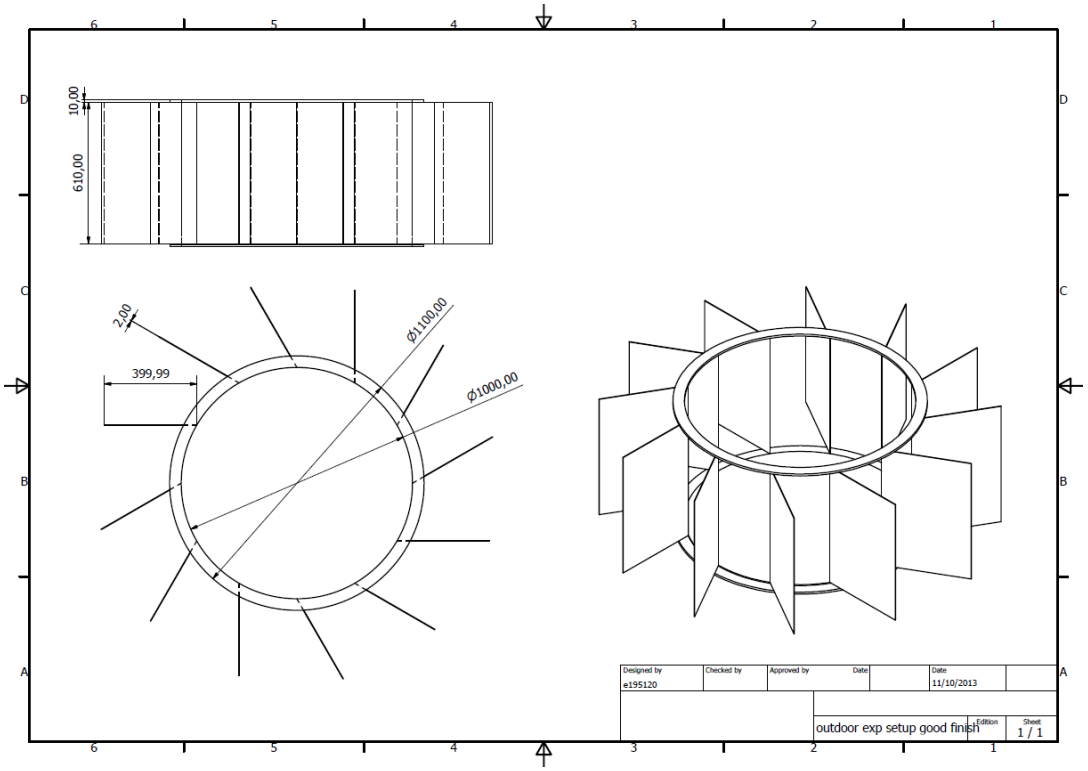

Figure 0.4 Technical drawing of the outdoor experimental setup

Another Meshing utility SnappyHexMesh that is used to import a CAD geometry and generate a mesh over the CAD geometry. A CAD geometry as shown in Figure 0.4 was exported in "stl" format and with the help of SnappyHexMesh dictionary mesh was generated.

A note on boundary condition at surface 4:

The boundary condition at the top surface 4 was selected to avoid convergence problems. The inflow from the surface 4 depends on the pressure drop at the center which is resulted by the

buoyant rising of the heated air. So the solver uses the pressure flux normal to the face to determine the inflow velocity.

APPENDIX B

THERMOPHYSICAL PROPERTIES

```
/*---------------------------*- C++ -*----------------------------*\
| =========                 |
|
| \\      /  F ield         | OpenFOAM: The Open Source CFD
Toolbox           |
|  \\    /   O peration     | Version:  2.1.0
|
|   \\  /    A nd           | Web:      www.OpenFOAM.org
|
|    \\/     M anipulation  |
|
\*-------------------------------------------------------------*/
FoamFile
{
    version     2.0;
    format      ascii;
    class       dictionary;
    location    "constant";
    object      thermophysicalProperties;
}
// * * * * * * * * * * * * * * * * * * * * * * * * * * * * * * * * *
//

thermoType
hRhoThermo<pureMixture<constTransport<specieThermo<hConstThermo<pe
rfectGas>>>>>;

pRef            100000;
mixture
{
    specie
    {
        nMoles          1;
        molWeight       28.9;
    }
    thermodynamics
    {
        Cp              1000;
        Hf              0;
    }
    transport
    {
```

```
        mu              1.8e-05;
        Pr              0.7;
    }}
/*--------------------------------*- C++ -*----------------------
*\
| =========                 |
|
| \\      /  F ield         | OpenFOAM: The Open Source CFD
Toolbox           |
|  \\    /   O peration     | Version:  2.1.x
|
|   \\  /    A nd           | Web:      www.OpenFOAM.org
|
|    \\/     M anipulation  |
|
\*---------------------------------------------------------------*/
FoamFile
{
    version     2.0;
    format      ascii;
    class       dictionary;
    object      transportProperties;
}

// * * * * * * * * * * * * * * * * * * * * * * * * * * * * * * * * *
//

transportModel Newtonian;

// Laminar viscosity
nu              nu [0 2 -1 0 0 0 0] 1e-05;

// Thermal expansion coefficient
beta            beta [0 0 0 -1 0 0 0] 3e-03;

// Reference temperature
TRef            TRef [0 0 0 1 0 0 0] 300;

// Laminar Prandtl number
Pr              Pr [0 0 0 0 0 0 0] 0.9;

// Turbulent Prandtl number
Prt             Prt [0 0 0 0 0 0 0] 0.7;

// ************************************************************* //
```

SAMPLE blockMesh DICTIONARY

```
/*--------------------*- C++ -*----------------------------*\
| =========                 |
|
| \\      /  F ield         | OpenFOAM: The Open Source CFD
Toolbox           |
|  \\    /   O peration     | Version:  2.1.0
|
|   \\  /    A nd           | Web:      www.OpenFOAM.org
|
|    \\/     M anipulation  |
|
\*---------------------------------------------------------------*/
FoamFile
{
    version     2.0;
    format      ascii;
    class       dictionary;
    object      blockMeshDict;
}
// * * * * * * * * * * * * * * * * * * * * * * * * * * * * * * * * *
//

convertToMeters 1;

 vertices
 (
(0 0 0)
(0.61 0 0)
(0 -0.129 0.482)
(0.61 -0.129 0.482)
(0.61 0.129 0.482)
(0 0.129 0.482)
(0 -0.0713 0.769)
(0 -0.446 0.630)
(0.61 -0.0713 0.769)
(0.61 -0.446 0.630)
(0 -0.300 1.097)
(0 -0.809 0.799)
(0.61 -0.300 1.097)
(0.61 -0.809 0.799)
(1.83 0 0)
(1.83 -0.129 0.482)
(1.83 0.129 0.482)
(1.83 -0.071 0.769)
(1.83 -0.446 0.630)
(1.83 -0.300 1.097)
```

```
(1.83 -0.809 0.799)
 );

edges
 (
arc 2 5 (0 0 0.50)
arc 3 4 (0.61 0 0.50)
arc 3 4 (1.83 0 0.50)
 );

 blocks
 (
  hex (0 1 1 0 2 3 4 5) (35 15 25) simpleGrading (2 1 1)
  hex (7 6 8 9 2 5 4 3) (15 35 15) simpleGrading (1 2 1)
  hex (11 10 12 13 7 6 8 9) (15 35 15) simpleGrading (1 2 1)
  hex (1 14 14 1 3 15 16 4) (5 15 25) simpleGrading (1 1 1)
  hex (9 8 17 18 3 4 16 15) (15 5 15) simpleGrading (1 1 1)
  hex (13 12 19 20 9 8 17 18) (15 5 15) simpleGrading (1 1 1)
 );

 patches
 (
         wall
         hot
         (
                 (0 5 2 0)
         )
         wall
         floor
         (
                 (2 5 6 7)
                 (11 10 6 7)
         )
         wall
         fixedWalls2
         (
                 (2 3 9 7)
                 (5 4 8 6)
         )
         patch
         ceiling
         (
                 (14 15 16 14)
                (15 16 17 18)
                (17 18 20 19)
         )

         cyclic
         fixedWalls1
         (
```

```
                (0 1 3 2)
                (7 9 13 11)
                (1 14 15 3)
                (3 15 18 9)
                (9 18 20 13)
                (0 1 4 5)
                 (6 8 12 10)
                (1 14 16 4)
                (4 16 17 8)
                (8 17 19 12)
        )
        patch
        hot2
        (
                (11 10 12 13)
                (13 12 19 20)
        )
);
```

APPENDIX C

fvSchemes dictionary

```
/*--------------------------*- C++ -*----------------------------*\
| =========                 |
|
| \\      /  F ield         | OpenFOAM: The Open Source CFD
Toolbox           |
|  \\    /   O peration     | Version:  2.1.x
|
|   \\  /    A nd           | Web:      www.OpenFOAM.org
|
|    \\/     M anipulation  |
|
\*---------------------------------------------------------------*/
FoamFile
{
    version     2.0;
    format      ascii;
    class       dictionary;
    location    "system";
    object      fvSchemes;
}
// * * * * * * * * * *  * * * * * * * * * * * * * * * * * * * * * //

ddtSchemes
{
    default         Euler;
}

gradSchemes
{
    default         Gauss linear;
}

divSchemes
{
    default         none;
    div(phi,U)      Gauss upwind;
    div(phi,T)      Gauss upwind;
    div(phi,k)      Gauss upwind;
    div(phi,epsilon) Gauss upwind;
    div(phi,R)      Gauss upwind;
    div(R)          Gauss linear;
    div((nuEff*dev(T(grad(U))))) Gauss linear;
```

```
}

laplacianSchemes
{
    default         none;
    laplacian(nuEff,U) Gauss linear uncorrected;
    laplacian((1|A(U)),p_rgh) Gauss linear uncorrected;
    laplacian(kappaEff,T) Gauss linear uncorrected;
    laplacian(DkEff,k) Gauss linear uncorrected;
    laplacian(DepsilonEff,epsilon) Gauss linear uncorrected;
    laplacian(DREff,R) Gauss linear uncorrected;
}

interpolationSchemes
{
    default         linear;
}

snGradSchemes
{
    default         uncorrected;
}

fluxRequired
{
    default         no;
    p_rgh;
}


// ************************************************************* //
```

APPENDIX D

fvSolution Dictionary

```
/*--------------------------*- C++ -*----------------------------*\
| =========                 |
|
| \\      /  F ield         | OpenFOAM: The Open Source CFD
Toolbox           |
|  \\    /   O peration     | Version:  2.1.x
|
|   \\  /    A nd           | Web:      www.OpenFOAM.org
|
|    \\/     M anipulation  |
|
\*---------------------------------------------------------------*/
FoamFile
{
    version     2.0;
    format      ascii;
    class       dictionary;
    location    "system";
    object      fvSolution;
}
// * * * * * * * * * * * * *  * * * * * * * * * * * * * * * * * * //

solvers
{
    p_rgh
    {
        solver          PCG;
        preconditioner  DIC;
        tolerance       1e-8;
        relTol          0.01;
    }

    p_rghFinal
    {
        $p_rgh;
        relTol          0;
    }

    "(U|T|k|epsilon|R)"
    {
        solver          PBiCG;
        preconditioner  DILU;
```

```
        tolerance       1e-6;
        relTol          0.1;
    }

    "(U|T|k|epsilon|R)Final"
    {
        $U;
        relTol          0;
    }
}

PIMPLE
{
    momentumPredictor no;
    nOuterCorrectors 1;
    nCorrectors     2;
    nNonOrthogonalCorrectors 0;
}

relaxationFactors
{
    fields
    {
    }
    equations
    {
        "(U|T|k|epsilon|R)" 1;
        "(U|T|k|epsilon|R)Final" 1;
    }
}
```